AD-A189 362 A PROTOTYPE WINDFLOW MODELING SYSTEM FOR TACTICAL 1/1
WEATHER SUPPORT OPERATIONS(U) AIR FORCE GEOPHYSICS LAB
HANSCOM AFB MA J M LANICCI ET AL 07 MAY 87
UNCLASSIFIED AFGL-RR-87-0159 F/G 4/2 NL

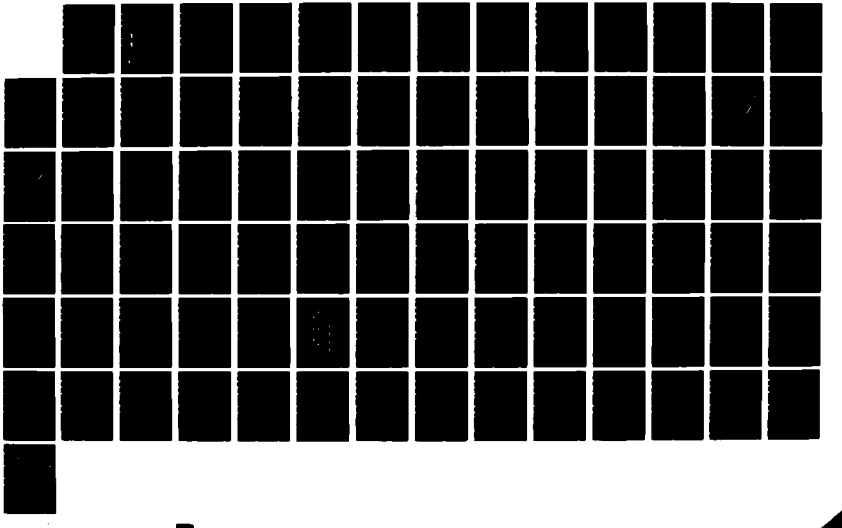

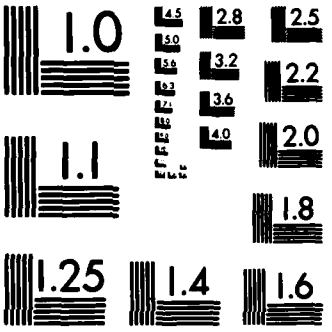

(4)

AFGL-TR- 87-0159
ENVIRONMENTAL RESEARCH PAPERS, NO. 975

A Prototype Windflow Modeling System for Tactical Weather Support Operations

JOHN M. LANICCI, CAPTAIN, USAF
JOAN M. WARD

7 May 1987

ATMOSPHERIC SCIENCES DIVISION PROJECT 6670

AIR FORCE GEOPHYSICS LABORATORY
HANSCOM AFB, MA 01731

This report has been reviewed by the ESD Public Affairs Office (PA) and is releasable to the National Technical Information Service (NTIS).

"This technical report has been reviewed and is approved for publication"

FOR THE COMMANDER

Donald D. Grantham

DONALD D. GRANTHAM
Chief, Atmospheric Structure Branch

Donald A. Chisholm for RAMc

ROBERT A. McCLATCHEY
Director, Atmospheric Sciences Division

Qualified requestors may obtain additional copies from the Defense Technical Information Center. All others should apply to the National Technical Information Service.

If your address has changed, or if you wish to be removed from the mailing list, or if the addressee is no longer employed by your organization, please notify AFGL/DAA, Hanscom AFB, MA 01731. This will assist us in maintaining a current mailing list.

Do not return copies of this report unless contractual obligations or notices on a specific document requires that it be returned.

Unclassified
SECURITY CLASSIFICATION OF THIS PAGE

REPORT DOCUMENTATION PAGE

Form Approved OMB No. 0704-0188

1a. REPORT SECURITY CLASSIFICATION: Unclassified	1b. RESTRICTIVE MARKINGS
2a. SECURITY CLASSIFICATION AUTHORITY	3. DISTRIBUTION/AVAILABILITY OF REPORT: Approved for public release; distribution unlimited.
2b. DECLASSIFICATION/DOWNGRADING SCHEDULE	
4. PERFORMING ORGANIZATION REPORT NUMBER(S): AFGL-TR-87-0159 ERP, No. 975	5. MONITORING ORGANIZATION REPORT NUMBER(S)
6a. NAME OF PERFORMING ORGANIZATION: Air Force Geophysics Laboratory 6b. OFFICE SYMBOL (If applicable): LYA	7a. NAME OF MONITORING ORGANIZATION
6c. ADDRESS (City, State, and ZIP Code): Hanscom AFB Massachusetts 01731-5000	7b. ADDRESS (City, State, and ZIP Code)
8a. NAME OF FUNDING/SPONSORING ORGANIZATION 8b. OFFICE SYMBOL (If applicable)	9. PROCUREMENT INSTRUMENT IDENTIFICATION NUMBER
8c. ADDRESS (City, State, and ZIP Code)	10. SOURCE OF FUNDING NUMBERS

PROGRAM ELEMENT NO.	PROJECT NO.	TASK NO	WORK UNIT ACCESSION NO.
62101F	6670	14	09

11. TITLE (Include Security Classification)
A Prototype Windflow Modeling System for Tactical Weather Support Operations

12. PERSONAL AUTHOR(S)
Lanicci, John M., Capt, USAF and Joan M. Ward*

13a. TYPE OF REPORT	13b. TIME COVERED	14. DATE OF REPORT (Year, Month, Day)	15. PAGE COUNT
Scientific. Interim.	FROM 86 Aug TO 87 Feb	1987 May 7	84

16. SUPPLEMENTARY NOTATION
*ST Systems Corp., Lexington, MA

17. COSATI CODES			18. SUBJECT TERMS (Continue on reverse if necessary and identify by block number)		
FIELD	GROUP	SUB-GROUP	Wind model	Surface layer	Tactical
0401			Complex terrain	Operational testing	weather
			Variational analysis	Wind profile	support

19. ABSTRACT (Continue on reverse if necessary and identify by block number)

This report documents the culmination of a three-year development and testing effort on a two-dimensional (x-y plane) surface-layer windflow model for complex terrain. The model was acquired from the U.S. Army Atmospheric Sciences Laboratory (ASL) at White Sands, New Mexico in 1984. The version of the model described in this report has been adapted to run using real time data on both the Zenith-100 and IBM-compatible Zenith-248 computers. The model accepts input of a single surface observation (or forecast) of wind, temperature, and cloud cover, and uses this information along with terrain information and the date/time to diagnose the surface-layer stability. The model then performs a variational analysis of the windfield, adjusting the winds through a relaxation technique until the windfield conforms to effects of topography, stability, ambient flow conditions, and mass continuity. The model is designed to produce high-resolution wind analyses, typically running on domains on the order of 10 × 10 km, with horizontal grid spacing of 100 to 200 m.

20. DISTRIBUTION/AVAILABILITY OF ABSTRACT	21. ABSTRACT SECURITY CLASSIFICATION
☐ UNCLASSIFIED/UNLIMITED ☒ SAME AS RPT. ☐ DTIC USERS	Unclassified

22a NAME OF RESPONSIBLE INDIVIDUAL	22b. TELEPHONE (Include Area Code)	22c OFFICE SYMBOL
John M. Lannici, Capt, USAF	(617) 377-2971	AFGL/LYA

DD Form 1473, JUN 86 *Previous editions are obsolete.* SECURITY CLASSIFICATION OF THIS PAGE
Unclassified

19. (Contd)

We present an overview of potential military and nonmilitary uses for the model, and describe the relevant physics and computer architecture of the model and its two utility plotting routines. A user's guide, included here as Section 4, is primarily aimed at providing operational users such as forecasters some guidelines for using the model and interpreting the output. Finally, we present the results of an operational test of the model in support of Army Special Forces operations at Ft. Devens, Massachusetts. The test results illustrate the model's potential as a tactical weather support tool for low-level aviation and paradrop activities.

Preface

The successful culmination of three years of model development and testing at AFGL does not happen without the contributions of countless individuals and organizations. Instead of describing these contributions in detail, we choose to list the individuals and groups who have helped us over the last several years:

Bruce Kunkel - AFGL
Harald Weber* - AFGL
Robert Banta - AFGL
AFGL Research Library
AFGL Photo Lab
AFGL Graphics
Ronald Cionco - ASL
William Ohmstede - Las Cruces, NM
Gordon Schacher - Naval Postgraduate School
Gail Vaucher - Naval Postgraduate School
HQ AWS, Scott AFB, IL
USAFETAC, Scott AFB, IL
HQ 5WW, Langley AFB, VA
HQ 5WS, Ft. MacPherson, GA
Science & Technology Corp., (Dr. Burlbaw)
Physical Science Laboratory, (Mr. Byers)
Defense Mapping Agency
HQ AFSC, Andrews AFB, MD (Capt Corley)
Capt Michael Buell - Det 30, 2WS Vandenberg AFB

Det 12, 5WS Ft. Devens:

Capt Wallace	SSgt Kielnecker
1Lt Huston	Sgt Alexander
MSgt Pukajlo	Sgt Wieand
TSgt Phillips	Sgt Caldwell

*Visiting scientist from German Military Geophysical Office, Traben-Trarbach FRG.

This manuscript was professionally typed by Mrs. Audrey Campana and Mrs. Anna Tortorici of AFGL.

Contents

Contents

Illustrations

Illustrations

Tables

A Prototype Windflow Modeling System for Tactical Weather Support Operations

1. INTRODUCTION

This report is the culmination of a three-year research effort at AFGL to develop and evaluate a two-dimensional (x-y plane) surface-layer windflow model for complex terrain. The report begins by outlining the operational need that exists today for accurate specification of the low-level windfield over irregular topography. The model physics and computer architecture are also described, as well as the peripheral programs used in the system. A user's guide is then presented, which is geared toward model usage by operational forecasters. We conclude with the results of an actual field test made with the model at the Air Weather Service (AWS) detachment at Ft. Devens, Massachusetts. The first section contains an overview of both the military and nonmilitary uses for the windflow modeling system, a summary of previous research efforts with the model, and instructions on the best utilization of the different sections of this report that are tailored to a variety of audiences.

1.1 Operational Need for Low-level Wind Information

The problem of specifying winds over irregular terrain embodies many physical considerations that impose difficulties on our ability to describe the flow accurately.

(Received for Publication 29 April 1987)

The presence of both natural and man-made obstacles over the land surface, the existence of nonhomogeneous vegetation and soils, bodies of water such as lakes and oceans, and the structure of the terrain itself, present a myriad of interacting and nonlinear physical processes that are difficult to specify and sort out. The advent of increasingly sophisticated numerical models has helped us in our understanding of which physical processes are important in the formation of slope winds, mountain-valley circulations, sea/land breezes over complex coastal regions, and the roles of these processes in convective cloud formation and creation of mesoscale circulations and boundaries. These models range in complexity from three-dimensional primitive-equation (PE) types such as the Penn State/NCAR model (Anthes and Warner[1]) and the Colorado State models (Mahrer and Pielke;[2] and Tripoli and Cotton[3]), to simpler single-layer models such as those of Danard,[4] Mass and Dempsey,[5] and Alpert et al.[6]

The above-mentioned models have been exclusively applied in research studies. Operationally-available numerical models have horizontal and vertical resolutions that are too coarse to resolve terrain-induced mesoscale systems such as mountain-valley circulations and slope flows (Pielke[7]). Obviously, the operational requirements for specifying wind conditions over a small region such as an individual mountain/valley system make the use of models that run on desktop computers an attractive option for those tasked with mesoscale weather forecasting duties. Such simple numerical models contain less physics than the larger, more complex PE models. This fact requires the forecaster to be more aware of the model limitations and makes the interpretation of the output a more difficult task.

---

1. Anthes, R.A., and Warner, T.T. (1978) The development of mesoscale models suitable for air pollution and other mesometeorological studies, Mon. Wea. Rev. 106:1045-1078.

2. Mahrer, Y., and Pielke, R.A. (1977) The effects of topography on sea and land breezes in a two-dimensional numerical model, Mon. Wea. Rev. 105:1151-1162.

3. Tripoli, G.J., and Cotton, W.R. (1982) The Colorado State University three-dimensional cloud/mesoscale 1982. Part I: General theoretical framework and sensitivity experiments, J. Rech. Atmos. 16:185-219.

4. Danard, M. (1977) A simple model for mesoscale effects of topography on surface winds, Mon. Wea. Rev. 105:572-581.

5. Mass, C.F., and Dempsey, D.P. (1985) A one-level, mesoscale model for diagnosing surface winds in mountainous and coastal regions, Mon. Wea. Rev. 113:1211-1227.

6. Alpert, P., Eppel, A., and Getenio, B. (1985) Surface wind prediction over complex terrain - Application of a one-level terrain following model to Israel, Preprints Seventh Conf. Numerical Weather Prediction, Am. Meteorol. Soc., Boston, Mass., pp. 369-373.

7. Pielke, R.A. (1982) The role of mesoscale numerical models in very-short-range forecasting, in Nowcasting, K.A. Browning, Ed., Academic Press Inc., New York.

The AFGL windflow modeling system described in this report was originally designed by Ball and Johnson[8] for use by the Army Atmospheric Sciences Laboratory (ASL) at White Sands, New Mexico, to specify terrain-induced wind effects over small areas of complex terrain (5 to 20 km on a side), using high horizontal resolutions typically between 100 and 200 m. The numerous mission support uses for such a model are described below:

(1) Low-level aviation—including close-air support missions, nap-of-the-earth helicopter flying, and low-level radar-avoidance flying by strategic forces. Other missions are low-level cargo delivery by transport aircraft, and approaches into and out of paradrop zones. Diagnosis of terrain-induced turbulence or wind effects in or around airfield locations is another potential use.

(2) Paradrop operations—a critical area that is very sensitive to strong or gusty surface winds and low-level wind shear. The setup of marker panels over the drop zone for the aircraft and jumpers is sensitive to wind direction and speed throughout the lowest 300 meters.

(3) Windflow climatology—useful for long- or short-range mission planning. This information is critical over data-denied or data-sparse areas. All aspects of mission planning such as target determinations, locations, favorable/unfavorable times, and go or no-go decisions are sensitive to this information.

(4) Target-acquisition winds—important for determining the types of weapons to use ("smart" and conventional). The model is especially useful for defining conditions on the enemy side of the forward edge of battle area (FEBA) and forward-line-of-own troops (FLOT).

(5) Nuclear, Biological, Chemical (NBC) Operations—this may be the most wind-sensitive operation of all since the transport and diffusion of contaminants can be affected by all aspects of the terrain and land surface. It is difficult to predict windflow for light wind situations in which the small-scale surface features such as vegetation, soil moisture, and slope aspect are important in producing certain flow patterns.

A considerable variety of nonmilitary uses for this type of model also exists. Several of these areas overlap or are complementary to the military uses described above, and thus need to be mentioned here:

---

8. Ball, J. A., and Johnson, S. A. (1978) Physically Based High Resolution Surface Wind and Temperature Analysis for EPAMS, ASL-CR-78-0043-1, U.S. Army Atmospheric Sciences Laboratory, White Sands Missile Range, New Mexico, ADA 055861.

(1) Transport and diffusion—obvious relationship to the NBC applications, especially for specifying hazard areas resulting from toxic chemical releases. Another area that has a military complement is fire weather, especially with regard to transport and diffusion of smoke, and spread of the fire (see Svejkovsky[9] for description of long-range smoke transport as detected from satellite).

(2) Agricultural meteorology—several applications in this area are frost prediction (inferred from examining cold-air drainage and pooling patterns), canopy effects on the windflow (see Cionco[10, 11] for descriptions of a canopy parameterization for the ASL version of the windflow model), soil erosion due to surface wind effects, and aerial spraying operations.

(3) Wind energy siting—specification of terrain-induced effects on the wind are important for locating wind energy sites since the windpower is proportional to the cube of the wind speed (Panofsky and Dutton[12]). Both numerical and empirical models have been used to examine this problem (Kirchoff and Kaminsky;[13] Barnard et al[14]).

(4) Civil aviation—low level aviation is sensitive to terrain effects on the wind, especially for gliders, light airplanes and helicopters.

(5) Numerical Weather Prediction (NWP)—models such as ours can be used in comparison studies with other, more complex models to explore the dominant physical processes present in terrain-induced flows.

---

9. Svejkovsky, J. (1985) Santa Ana airflow observed from wildfire smoke patterns in satellite imagery, Mon. Wea. Rev. 113:902-906.

10. Cionco, R.M. (1983) On the coupling of canopy flow to ambient flow for a variety of vegetation types and densities, Boundary - Layer Meteorol. 26:325-335.

11. Cionco, R.M. (1985) On modeling canopy flow coupled to the surface boundary layer, Proc. 17th Conf. on Agriculture and Forest Meteorology and 7th Conf. on Biometeorology and Aerobiology, Am. Meteorol. Soc., Boston, Mass., pp. 116-119.

12. Panofsky, H.A., and Dutton, J.A. (1984) Atmospheric Turbulence: Models and Methods for Engineering Applications, Wiley, New York, 297 p.

13. Kirchoff, R.H., and Kaminsky, F.C. (1983) Empirical Modeling of Wind Speed Profiles in Complex Terrain, DOE-ET/10374-82/1 (DE 83011613), Pacific Northwest Laboratory (Contract DE-AC06-76RLO 1830), Richland, Wash., 99352.

14. Barnard, J.C., Wegley, H.L., and Hiester, T.R. (1985) Improving the Performance of Mass-Consistent Numerical Models Using Optimization Techniques, PNL-5566 (Contract DE-AC06-76RLO 1830), Pacific Northwest Laboratory, Richland, Wash., 99352.

A windflow model analysis can be used to initialize a high-resolution PE model for areas of complex terrain where an objective analysis is unsuitable. Prediction of other weather phenomena such as radiation fog could be accomplished by examining cold-air drainage patterns to infer or actually calculate temperature and moisture distributions (Tabony[15]).

1.2 Previous Work With the Model

The research and development involving this model over the last eight years has mainly centered on parallel efforts at ASL and AFGL.

At ASL, the model has been employed in conjunction with a pseudo-particle diffusion model to study the dispersion of smoke in battlefield environments (Cionco;[16] Ohmstede;[17] and Ohmstede and Stenmark[18]). Further development of the windflow model was done by Amlicke and Coleman,[19] who examined the way the model determines the exponent for the power-law wind profile, and created a capability for the model to be initialized with the modified output from a larger-scale numerical model. Cionco[10,11] described the coupling of a vegetative canopy formulation to the model, and documented the windflow model's place in ASL's model hierarchy (Cionco[20]). The ASL model hierarchy is a system of numerical models that covers the mesoscale from horizontal scales of 200 km down to 5 km. Veazey and Tabor[21] used the windflow model to examine requirements for meteorological sensor density on the battlefield.

---

15. Tabony, R.C. (1985) Relations between minimum temperature and topography in Great Britain, J. Climatology 5:503-520.

16. Cionco, R.M. (1982) A meteorological approach to chemical defense over complex terrain with vegetation, Workshop on the Parameterization of Mixed-Layer Diffusion, Las Cruces, N. Mex., pp. 323-328.

17. Ohmstede, W.D. (1982) The parameterization of battlefield dispersion-new frontiers, Workshop on the Parameterization of Mixed-Layer Diffusion, Las Cruces, N. Mex., pp. 279-287.

18. Ohmstede, W.D., and Stenmark, E.B. (1982) A model for characterizing transport and diffusion of air pollution in the battlefield environment, Workshop on the Parameterization of Mixed-Layer Diffusion, Las Cruces, N. Mex., pp. 416-423.

19. Amlicke, B.B., and Coleman, I.W. (1984) High Resolution Wind (HRW) Model, MRC/WDR-R-089, Mission Research Corporation, Alexandria, VA.

20. Cionco, R.M. (1985) Modeling airflow over variable terrain, Proc. of the HAZMAT '85 West Conference, Long Beach, Calif.

21. Veazey, D.R., and Tabor, P.A. (1985) Meteorological sensor density on the battlefield, Workshop on Geographic Information Systems in Government, Bruce Opitz (Ed.), Deepak Publishing, Hampton, VA, pp. 195-208.

The model was acquired by AFGL in 1984 for incorporation into a toxic chemical prediction system for complex terrain (Weber[22]). It has been used to study the sensitivity of surface-layer flow to the horizontal distribution of vegetative cover under various stability conditions (Lanicci[23]). A real-data study was performed on the model using meteorological tower data from Vandenberg AFB, California (Lanicci and Weber[24]). Further model developments at AFGL included the creation of different meteorological data input options (including a cursory objective analysis for multiple observations), and the adaptation of the code to small computers such as the Zenith-100. The model has been applied to various types of terrain, including gentle topography with complex vegetation cover (Ft. Polk, Louisiana), rough terrain with sparse vegetation (Vandenberg), and rolling terrain with fairly uniform forest cover (Ft. Devens, Massachusetts).

1.3 How to Use This Report

We have designed this report to be as comprehensive as possible in the documentation of the modeling system. Since it is nearly impossible to present a text that is universally applicable to operational and research people alike, we have designated separate sections aimed at different readers.

The AFGL windflow modeling system is available for varied groups to use for the many applications described in Section 1.1. Researchers will find Sections 1, 2, 3 and possibly Section 5 to be most useful to them. Computer scientists who are primarily programmers will most likely have use for the flowcharts and subroutine descriptions in Section 3, and find Section 4 useful if they do not have a meteorological background but wish to understand how the model works. Operational users such as weather forecasters will find Section 1.1 to be helpful, as well as Sections 4 and 5, and the descriptions of the Ft. Devens case studies in Appendix A. Anyone wanting to develop this system further, or use the system for their own operational purposes will want to read this entire report.

---

22. Weber, H. (1986) private communication.

23. Lanicci, J.M. (1985) Sensitivity Tests of a Surface-Layer Windflow Model to Effects of Stability and Vegetation, AFGL-TR-85-0265, ADA 169136.

24. Lanicci, J.M., and Weber, H. (1986) Validation of a Surface-Layer Windflow Model Using Climatology and Meteorological Tower Data from Vandenberg AFB, California, AFGL-TR-86-0210, ADA 178480.

The guidelines on the preceding page are just suggestions. We hope they are useful to those readers who may be unfamiliar with models of this type and need some direction in finding out more about our system in the least confusing manner.

2. THE MODEL AND ITS PHYSICS

The basic theory and equations for the windflow model are contained in Ball and Johnson,[8] Amlicke and Coleman,[19] and Lanicci.[23] We present here a summary of the theoretical framework surrounding the model equations and an outline of the model's iterative procedure to arrive at its windflow analysis.

2.1 Variational Analysis Theory

The theoretical basis for the model equation is Gauss' Principle of Least Constraint. The essence of the theory is that the motion that occurs in nature takes place in such a way as to minimize constraint forces arising from kinematic conditions. In order to better understand Gauss' principle, we proceed through the following analyses taken from Lanczos,[25] and Ball and Johnson.[8]

2.1.1 FOR A SYSTEM OF POINT PARTICLES

We begin with D'Alembert's Principle of Virtual Work, which states that any system of forces is in equilibrium if we add the inertial (created by the motion) forces to the impressed forces:

$$\sum_{k=1}^{N} (F_k - m_k \vec{A}_k) \cdot \delta R_k = 0 , \qquad (1)$$

where the summation is taken over the system of N particles, $\vec{F}_k \cdot \delta R_k$ is the virtual work done on a system by the impressed forces, and $-m_k \vec{A}_k$ is the inertial force.

Gauss applied D'Alembert's principle at time $t + \tau$ where τ is an arbitrarily small time interval, thus choosing $\delta \vec{R}(t + \tau)$ to be embodied as a variation in the acceleration $\vec{A}$:

$$\delta \vec{R}(t+\tau) = 1/2\, \delta \vec{A}(t) \cdot \tau^2 . \qquad (2)$$

---

25. Lanczos, C. (1970) The Variational Principles of Mechanics (4th Ed.) U. of Toronto Press, Toronto, pp. 106-110.

which is derived from Taylor's expansion of the particle path deviation $\delta \vec{R}_k$. We rewrite Eq. (1) as:

$$\sum_{k=1}^{N} (\vec{F}_k - m_k \vec{A}_k) \cdot \delta \vec{A}_k = 0 . \tag{3}$$

Since $\vec{F}_k$ is given and cannot be varied, we can rewrite Eq. (3) as shown below:

$$\sum_{k=1}^{N} (\vec{F}_k - m_k \vec{A}_k) \cdot \delta \frac{(\vec{F}_k - m_k \vec{A}_k)}{m_k} = 0 , \tag{4}$$

then applying the derivative rule for the quantity in Eq. (4) yields:

$$\delta \sum_{k=1}^{N} \frac{1}{2m_k} (\vec{F}_k - m_k \vec{A}_k)^2 = 0 . \tag{5}$$

Gauss redefined Eq. (5) as follows:

$$Z = \sum_{k=1}^{N} \frac{1}{2m_k} (\vec{F}_k - m_k \vec{A}_k)^2 , \tag{6}$$

where the quantity Z is defined as the "constraint" of the motion. The principle in Eq. (6) says that motion occurring in nature seeks to minimize Z. If there are no constraints, Z = 0, and Eq. (6) is reduced to Newton's Law of Motion. This principle is exactly analogous to the Principle of Least Squares or Least Action that forms the basis for many variational analysis schemes that seek to minimize the difference between a theoretical value of a function and its observed value. See the discussions by Sasaki,[26, 27] and Haltiner and Williams,[28] for examples of the application of the Least Squares principle to numerical analysis.

---

26. Sasaki, Y. (1958) An objective analysis based on the variational method, J. Meteorol. Soc. Japan 36:77-88.

27. Sasaki, Y. (1970) Some basic formalisms in numerical variational analysis, Mon. Wea. Rev. 98:875-883.

28. Haltiner, G.J., and Williams, R.T. (1980) Numerical Prediction and Dynamic Meteorology (2nd Ed.), Wiley and Sons, New York, 447 p.

2.1.2 FLUID MECHANICS ANALOGY

Within the realm of fluid mechanics, there have been several applications of a least action principle approach to describing fluid motion. Dutton[29] presented a derivation of the meteorological equation of motion using a least action approach. The constraints imposed upon the system were isentropic motion (an energy constraint) and inviscid conditions. We present the results of his derivation below [his Eq. (16) in Chapter 11, Section 5]:

$$\Delta A = - \int\int \rho \delta \vec{x} \cdot \left(\frac{\partial \vec{v}}{\partial t} + \vec{v} \cdot \nabla \vec{v} + \frac{1}{\rho} \nabla \rho + \nabla \Phi \right) dV\, dt$$

$$- \int\int \rho T \delta s \, dV\, dt \, , \qquad (7)$$

where ΔA is the variation of the action A of the system, ρ is the density, $\vec{v}$ is the wind velocity vector, p is pressure, Φ is the geopotential (potential energy of a unit mass in the earth's gravity field), T is the temperature, and δs is the variation of specific entropy s. Equation (7) contains two integrals over the fluid volume and time, and Dutton states that for isentropic motion, $\delta s = 0$, thus leaving only the first integral. For the action A to be a minimum, ΔA must vanish for arbitrary variation $\delta \vec{x}$ vanishing outside the time interval t_o, t_1, and on the fluid boundaries. This condition necessitates that the quantity in parentheses in Eq. (7) vanish, which is the equation of motion. Dutton's derivation demonstrates, from an energetics approach, that the atmospheric kinetic energy is only as large as is needed to respond to external forces acting upon it.

Ball and Johnson[8] took another approach in describing the fluid motion by applying Gauss' Principle of Least Constraint to incompressible, inviscid flows:

$$\delta \int_V \frac{\rho}{2} (\vec{A} + \vec{g})^2 \, dV \; - \delta \int_S \tau \vec{A} \cdot d\vec{s} = 0 \, , \qquad (8)$$

where $\vec{A}$ represents the fluid acceleration, $\vec{g}$ is gravity (an external force), and τ is the scalar stress in the outward normal direction to the surface s. These two integrals are taken over the fluid volume and its boundary surface, respectively. Notice the similarity between the volume integral in Eq. (8) and the formulation for point particles shown in Eq. (5). By applying the incompressibility assumption through introduction of Lagrange multipliers λ and applying some manipulations to Eq. (8), Ball and Johnson produce a form of the Gaussian principle shown below [see their Eqs. (II.2) and following]:

---

29. Dutton, J. A. (1976) The Ceaseless Wind, McGraw-Hill, New York, pp. 435-439.

$$\int_V (\vec{A} + \vec{g} + \frac{1}{\rho} \nabla\lambda) \cdot \delta\vec{A}\, dV - \int_S \frac{1}{\rho} (\tau + \lambda)\, \delta\vec{A} \cdot d\vec{s} = 0 . \qquad (9)$$

We can expand Eq. (9) and set $\lambda = p$ (the pressure) to produce another form:

$$\int_V (\frac{\partial\vec{v}}{\partial t} + \vec{v} \cdot \nabla\vec{v} + \vec{g} + \frac{1}{\rho} \nabla p) \cdot \delta\vec{A}\, dV - \int_S \frac{1}{\rho} (\tau + p)\, \delta\vec{A} \cdot d\vec{s} = 0 . \qquad (10)$$

Notice from Eq. (10) that the term in the parentheses of the volume integral represents the equation of motion. Notice that the minimum constraint presented here corresponds to a situation where the equation of motion and the kinematic constraint are both satisfied. The pressure gradient term in Eq. (10) results from the condition of incompressibility, thus making the pressure gradient a force of constraint arising from incompressibility.

To apply Gauss' principle to the surface layer, Ball and Johnson assumed that the fluid volume is a single layer, and introduced some simplifying assumptions to derive the basic windflow model equation. The first of these is the introduction of a Boussinesq approximation to characterize the external force $\vec{g}$ as a buoyancy force $\vec{B}$, defined in Eq. (11):

$$\vec{B} = \rho'\vec{g}/\rho_o , \qquad (11)$$

where ρ' is the density perturbation from its ambient value ρ_o. This assumption along with the Archimedean principle, allows the buoyancy force to be described using the potential temperature θ instead of density:

$$\vec{B} = \frac{\vec{g}\rho'}{\rho_o} = \frac{\vec{g}\theta'}{\theta_o} = \vec{g}\, \frac{(\theta_o - \theta_s)}{\theta_o} , \qquad (12)$$

where θ_s is the surface potential temperature, and θ_o is a reference potential temperature above the surface. Since we want to apply these relations to the surface layer, θ_o should be chosen so that $(\theta_o - \theta_s)$ accurately represents the surface-layer stability. The Boussinesq assumptions can be applied to Eq. (8) with the following result:

$$\delta \int_V \frac{\rho_o}{2} \left[\vec{A} + \vec{g}\, \frac{(\theta_o - \theta_s)}{\theta_o}\right]^2 dV + \delta \int_S p'\, \vec{A} \cdot d\vec{s} = 0 . \qquad (13)$$

We have also introduced the dynamic pressure p' in the surface integral as an additional external force. The next simplification into the system is the introduction of terrain-following coordinates. This allows some terms in Eq. (13) to be discarded in the application to the single-layer representation. A no-slip condition at the surface [$\vec{V}(Z = 0) = 0$] means that the only contribution to the surface integral in Eq. (13) is from the upper boundary, which is the boundary between the surface layer and atmospheric layers above. Since the model only considers a single layer, the surface integral and any surface normal components of the volume integral are discarded as a modeling approximation, leading to the following equation:

$$\delta \int_V \left[\vec{A} + \vec{g}_{11} \frac{(\theta_o - \theta_s)}{\theta_o} \right]^2 dV = 0 , \qquad (14)$$

where the "11" denotes surface parallel components. The surface-parallel components of buoyancy in Eq. (14) result in the introduction of horizontal temperature gradients, which in turn introduce a horizontal pressure gradient force, the latter force being one of the driving mechanisms involved in slope flows (Atkinson[30]). The expression in Eq. (14) can be redefined in the same fashion as Eq. (5) was, producing the basic model equation shown below:

$$R_t = \int_V \left[\vec{A} + \vec{g}_{11} \frac{(\theta_o - \theta_s)}{\theta_o} \right]^2 dV , \qquad (15)$$

where R_t is the total constraint R over the modeled volume, that is to be minimized by the integration of Eq. (15). One final note about Eq. (15) is the assumption of steady-state conditions (that is, $\frac{\partial \vec{V}}{\partial t} = 0$) in the momentum field. This means that only the advection $\vec{V} \cdot \nabla \vec{V}$ contributes to the acceleration term $\vec{A}$. This assumption means that the windflow model is essentially an analysis tool, the implications of which are further explored in Section 2.3.

2.2 Relaxation Procedure and Physical Parameterizations

Having established the basic model equation [Eq. (15)], we now describe the means by which the minimum constraint R_t is reached. The version of the model described in this report uses a single surface observation of wind direction and speed, temperature, and cloud cover, along with date and time, to initialize the

30. Atkinson, B. W. (1981) Mesoscale Atmospheric Circulations, Academic Press, London, pp. 252-254.

model with a uniform windfield and buoyancy. The model produces its terrain-induced windflow analysis through a relaxation procedure, incrementally adjusting the initially uniform windfield at each grid point every iteration step. The iterative procedure continues in the model until the first minimum of R_t over the domain is achieved. Numerical experiments performed by Lanicci and Weber[24] over artificial terrain showed that integration of the model equation beyond the first R_t minimum produced oscillations in R_t, eventually reaching a near-absolute minimum after about 195 steps. However, the resultant windfield analysis is a pure slope-wind solution that is independent of the ambient initial wind speeds. Therefore, the first or local R_t minimum is used as the point at which the model integration procedure stops, as it produces a solution that is meterologically consistent, having well-integrated the effects of topography, stability, mass conservation, and momentum advection. The relaxation procedure is described by the flow chart in Figure 1.

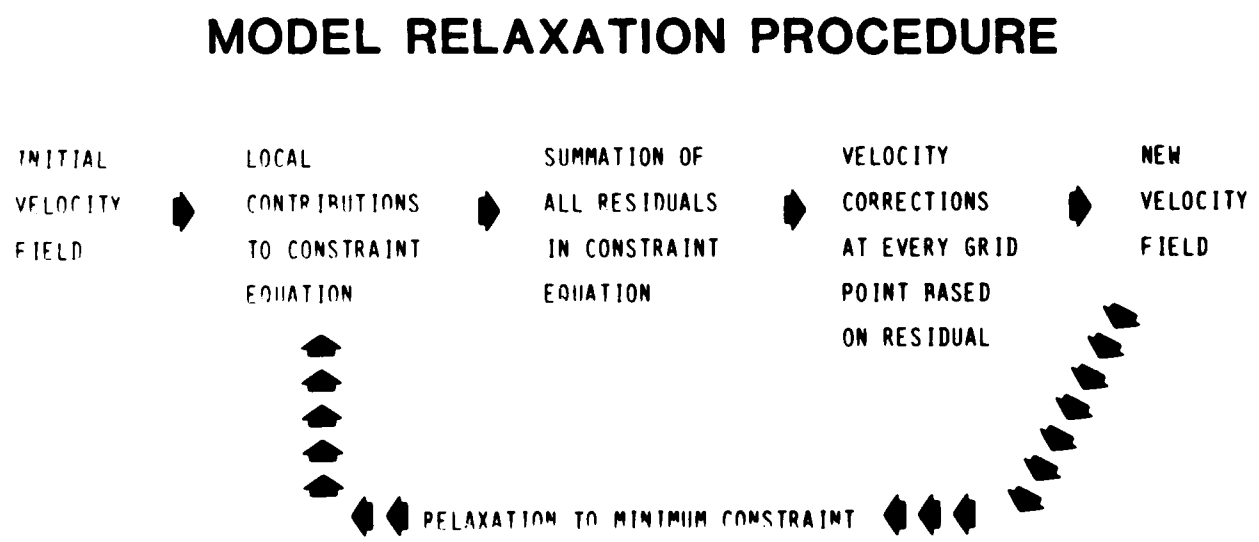

Figure 1. Flowchart Depicting Iterative Procedure by Which Model Tries to Minimize Constraint in Eq. (15)

The terrain-following coordinate system employed in the model uses a staggered grid system. Terrain elevations are on one set of grid points, with wind calculation grid points staggered in between, so that calculated terrain slopes can be used in the model integration. The single-layer formulation of the model is represented by using the flux form of the momentum advection in Eq. (15). The

model calculates momentum flux through boxes of thickness z_c, whose corners correspond to the terrain grid points. A schematic diagram of these flux box elements on the model domain is shown in Figure 2. The momentum flux through each face of the flux box is calculated and modified by the effects of the local surface-layer stability to determine the contribution of each flux box element to the $\vec{A}$ term of Eq. (15).

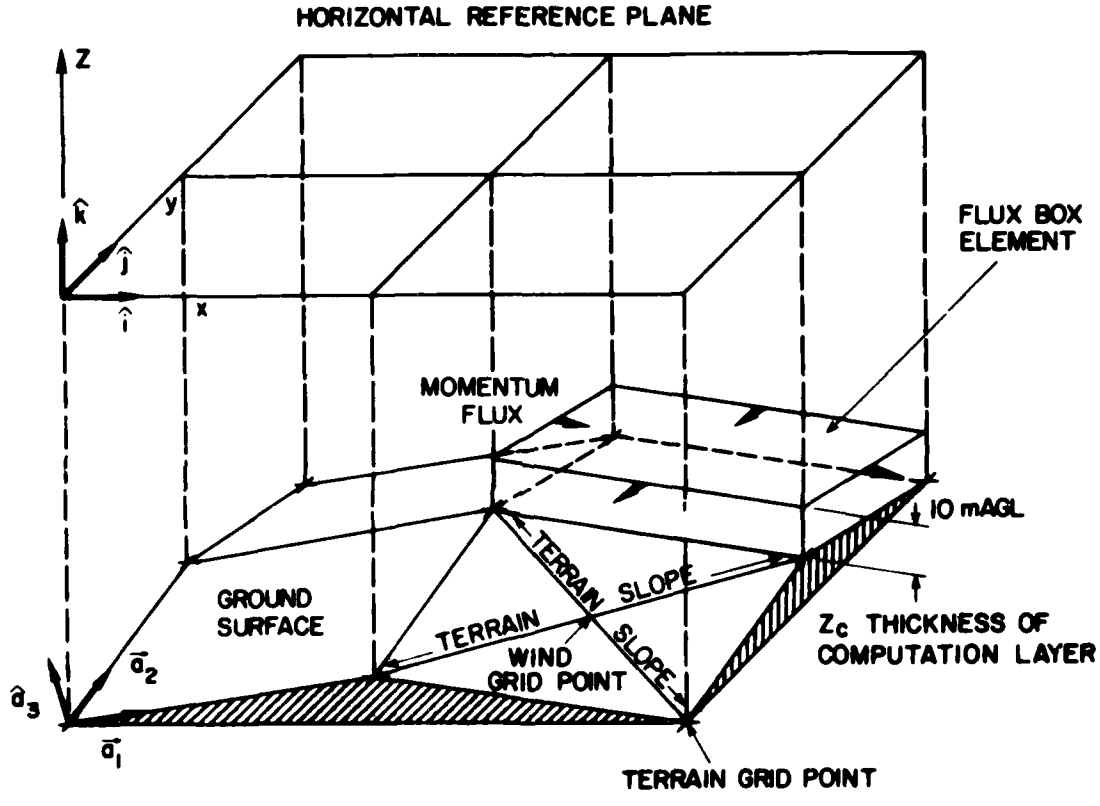

Figure 2. Diagram Showing Grid Structure and Geometry of Model Domain, With Structure of Individual Flux Box. Notice that the staggered grid system allows terrain slopes centered on the wind grid points to be integrated into model calculations, through the terrain-following coordinate axes a_1 and a_2 (after Ball in Johnson[8])

The basis for determining the surface-layer stability is the original calculation of the buoyancy term $\vec{B}$, using the surface observation to diagnose a stability

class based on a Pasquill-type category formulation (Turner[31]). Kunkel[32] devised a continuous stability parameter SP for the AFGL diffusion model that we have adapted for diagnosing stability in the windflow model. The stability parameter is analogous to the Pasquill category, but its use avoids sudden changes in stability and thus hazard distance, with slight changes in windspeed, solar elevation angle, or cloud cover. The values of SP range from 0.5 (unstable-Pasquill category A) to 6.0 (stable-Pasquill category F), and their relationship is illustrated in Table 1.

Table 1. Relation Between the Pasquill Stability Categories (SC) and the Continuous Stability Parameter (SP). (After Kunkel)[32]

SC	A	B	C	D	E	F
SP	0.5-1	1-2	2-3	3-4	4-5	5-6

The scheme for calculating SP based upon the surface observation is described in detail by Kunkel.[32] We summarize the method using the flowchart of Figure 3. The latitude, longitude, date, and time are used to determine incoming solar radiation as a function of solar elevation angle, according to:

$$I = S_o (t_1 - t_o) \sin(A)\, \tau^{\csc(A)} \qquad (16)$$

where I is the incoming solar radiation over a unit horizontal area on the earth's surface during time $(t_1 - t_o)$, S_o is the solar constant (1353.3 Wm^{-2}), A is the solar elevation angle, and τ is the atmospheric transmission coefficient (set equal to 0.7 in the model). Also notice from Figure 3 that the presence of clouds enters into the stability calculation in two ways. The first way is during the day, when a cloud cover of 7/8 or 8/8 (overcast conditions) causes the I calculation in Eq. (16) to be modified by the presence of different types of clouds, using the formulations contained in Table 17 of the Smithsonian Meteorological Tables.[33] The second way

31. Turner, D.B. (1964) A diffusion model for an urban area, J. Appl. Meteorol. 3:83-91.

32. Kunkel, B.A. (1985) Development of Atmospheric Diffusion Model for Toxic Chemical Releases, AFGL-TR-85-0338, ADA 169135.

33. List, R.J., Ed. (1985) Smithsonian Meteorological Tables (Vol. 114) Smithsonian Miscellaneous Collections.

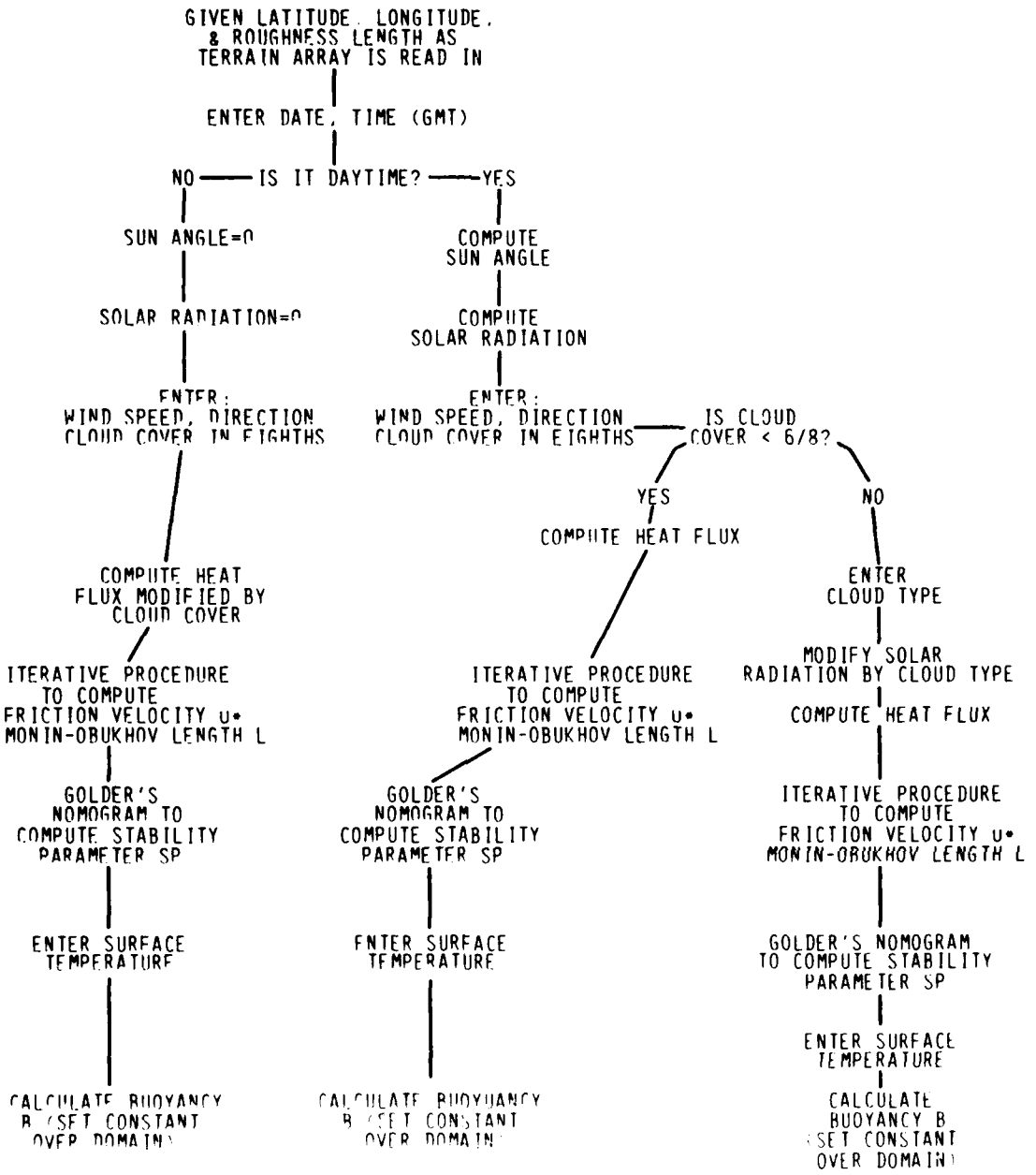

Figure 3. Flowchart Describing Procedure for Model Diagnosis of Stability Parameter and Buoyancy Magnitude, Using Input of Surface Observation

is at night, when the cloud cover modifies the computation of surface heat flux H through the relation shown in Eq. (17) (after Smith[34]):

34. Smith, F. B. (1972) A scheme for estimating the vertical dispersion of a plume from a source near ground level, Proc. of the Third Meeting of the Expert Panel on Air Pollution Modeling, NATO Committee on the Challenges of Modern Society, Paris, France.

$$H = H_o (1 - c/8), \tag{17}$$

where $H_o = -40\ Wm^{-2}$ (downward nighttime heat flux in the model), and c is the cloud cover (varying from 0 to 8). During the daytime, the formula for H becomes:

$$H = 0.4 (I - 100), \tag{18}$$

Using the I value computed from Eq. (16). An iterative procedure to calculate friction velocity u_* and Monin-Obukhov length L is then performed, using formulas from Ragland and Dennis[35] based on different magnitudes of H. Once the values of u_* and L have been determined by the appropriate formulas, the stability parameter SP is computed by applying the nomogram defined by Golder,[36] as put in equation form by Kunkel[32]:

$$SP = A + B \log Z_o, \tag{19}$$

where A and B are constants that are functions of 1/L and Z_o is the surface roughness length. We should note here that Z_o is constant over the model domain in the version described in this report. If one desires to use a nonhomogeneous Z_o, an appropriate value must be chosen for use in Eq. (19), or one could apply Eq. (19) at every grid point, using the individual grid value of Z_o, that would yield values of SP over domain as a function of nonhomogeneous surface roughness. Once SP has been determined by Eq. (19), the buoyancy $\vec{B}$ can be calculated using a form of Eq. (12) modified for use of temperature instead of potential temperature:

$$\vec{B}_{11} = \vec{g}\ \frac{(\Delta T + \gamma \Delta Z)}{T_s + \Delta T} \tag{20}$$

where ΔT is the vertical temperature change over depth ΔZ (100 m), γ is the adiabatic lapse rate ($\simeq 1.0°C\ 100\ m^{-1}$), and T_s is the surface temperature in K. The vertical temperature change ΔT is a function of SP, and they are related to each other through the values found in U.S. NRC Regulatory Guide 1.23,[37] and

35. Ragland, K.W., and Dennis, B.L. (1975) Point source atmospheric diffusion model with variable wind and diffusivity profiles, Atmos. Environ., 9:175-189.

36. Golder, D. (1972) Relations among stability parameters in the surface layer, Boundary Layer Meteorol. 3:47-58.

37. USNRC (1972) Onsite Meteorological Programs Regulatory Guide 1.23, U.S. Nuclear Regulatory Commission.

summarized by Table 1 in Sedefian and Bennett.[38] Figure 4 shows a graph relating SP to the actual lapse rate $\Delta T/\Delta Z$ (solid curve). The model uses an exponential equation fit to this curve, that is described by the dashed curve in Figure 4.

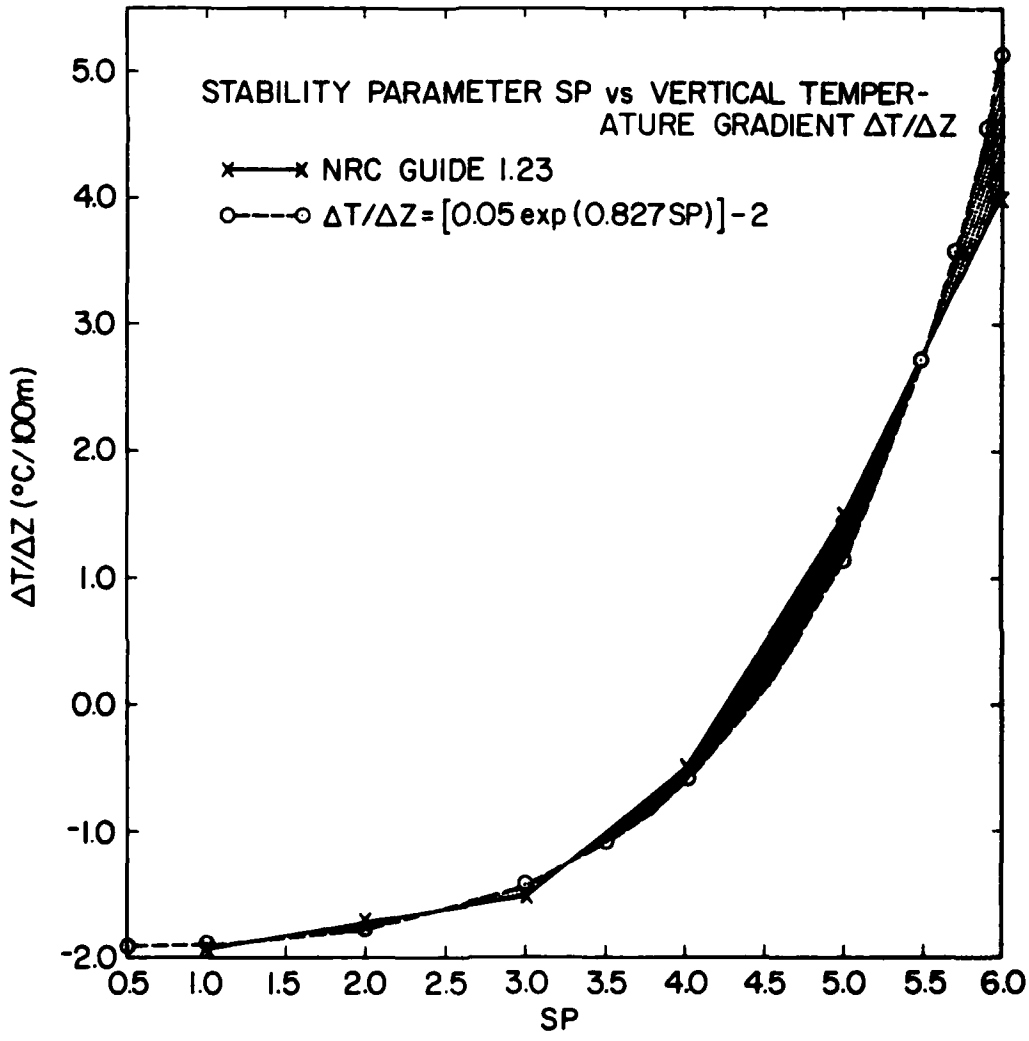

Figure 4. Graph Showing Stability Parameter SP vs Vertical Temperature Gradient (°C 100 m^{-1}) From NRC Guide (solid line) and Model Equation Fit (dashed line). Differences between the two curves are shown by stippling. Model overestimates of the magnitude of $\Delta T/\Delta Z$ are shown by light stippling, underestimates by dark stippling

38. Sedefian, L., and Bennett, E. (1980) A comparison of turbulence classification schemes, Atmos. Environ. 14:741-750.

The shaded areas show the differences between the exponential formulation and the NRC Guide values of $\Delta T/\Delta Z$ vs SP. The largest discrepancies are for stability parameters approaching 6.0, where the model curve overestimates $\Delta T/\Delta Z$ by as much as 1°C. Despite these differences, the correlation coefficient for the model equation is around 0.99. More important than these discrepancies in $\Delta T/\Delta Z$ are those in buoyancy magnitude B as a result of the exponential curve fit. These differences are highlighted in Figure 5, which shows B as a function of SP for the NRC table (solid curve), and for the exponential solution from Figure 4. As in Figure 4, the largest discrepancies appear for stable cases as SP approaches 6.0. These differences are only as large as 0.035 ms^{-2}, and since Lanicci[23] found that the model windfields are not as sensitive to the buoyancy magnitude as they are to its sign, we believe that this curve fit is adequate for diagnosing stability conditions in the model.

Once the buoyancy has been computed, it remains constant over the domain throughout the entire integration. However, the local surface-layer stability at each grid point is determined by calculating the value of a power-law wind profile exponent. This procedure is summarized by the upper flowchart shown in Figure 6. The wind profile exponent n is influenced by the surface-layer stability, using the equation below (after Panofsky and Dutton[12]):

$$n = \phi_m / [\ln \bar{Z}/Z_o) + \psi_m] , \tag{21}$$

where ϕ_m is the Monin-Obukhov nondimensional vertical wind shear, and ψ_m is a Monin-Obukhov function dependent upon 1/L. The values of ϕ_m and ψ_m are determined through use of the Businger et al[39] profiles at each grid point. The value of $\bar{Z}$ is determined by adding Z_o to the model calculation height, set at 10 m above ground. Since we are interested in windflow close to the surface, 10 m is a good calculation height to use since the flow at this level is often strongly influenced by surface features (Panofsky and Dutton[12]). The upper flowchart in Figure 6 shows how the bulk Richardson number Ri_b determines the stability regime used to calculate appropriate values of ϕ_m, ψ_m, and thus n. The Ri_b formula used in this model is shown below:

$$Ri_b = B\bar{Z}/u^2 , \tag{22}$$

---

39. Businger, J.A., Wyngaard, J.C., Izumi, Y., and Bradley, E.F. (1971) Flux-profile relationships in the atmospheric boundary layer, J. Atmos. Sci. 28:181-189.

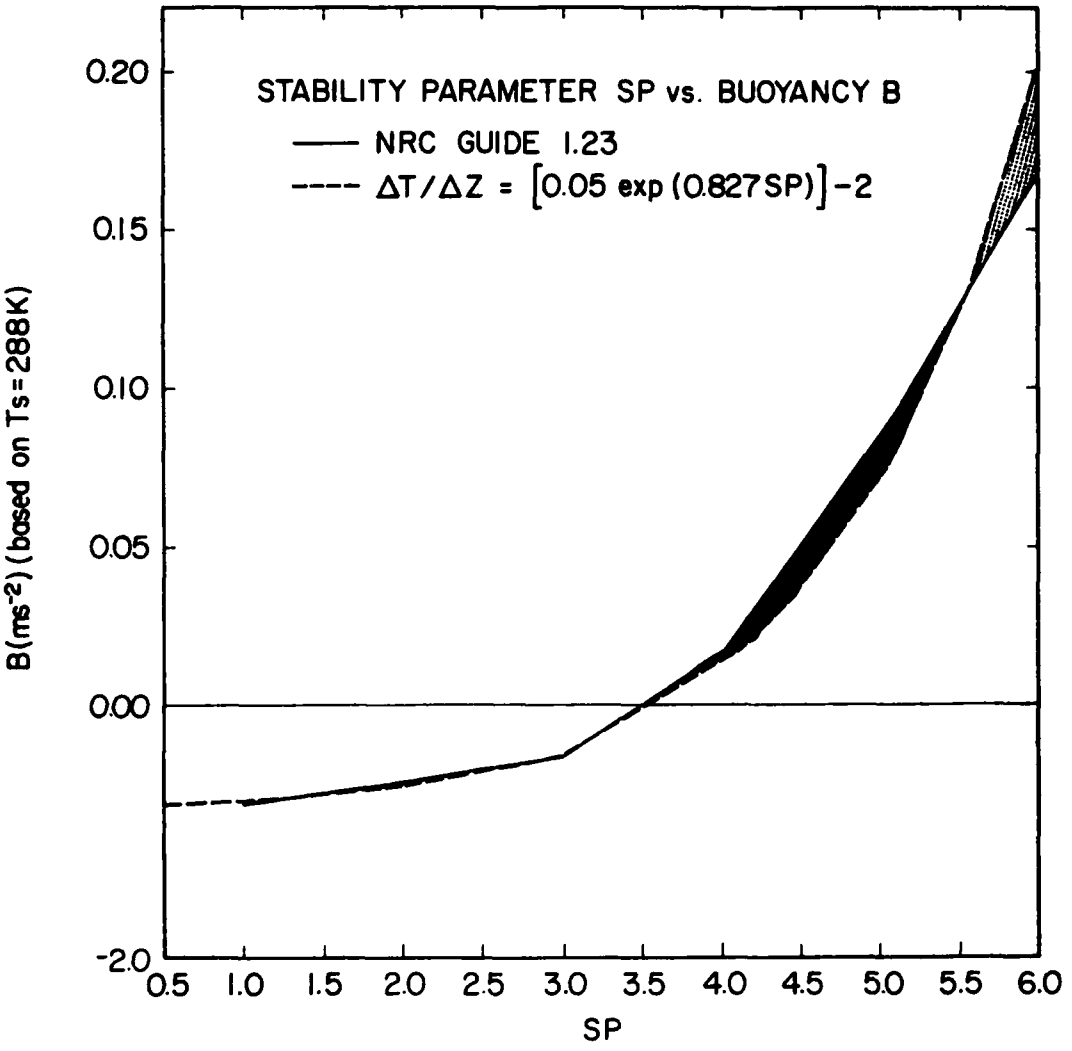

Figure 5. Graph Relating Stability Parameter SP vs Buoyancy Magnitude for NRC Guide (solid line) and Model Equation Fit (dashed line). Differences between the two curves are highlighted by stippling as in Figure 4

where u is the windspeed. Several points should be made about the methodology described in Figure 6. First, the Ri_b value can change as u is adjusted at each grid point, even though B remains constant. Second, the use of Monin-Obukhov scaling parameters in determining n is consistent with using the same scaling relationships in computing B. Since the assumption of a constant B over the domain is only an approximation, we allow local stability effects to affect the model wind solution using the procedure described in the bottom flowchart of Figure 6. Thus the calculation of local grid values of Ri_b, ϕ_m, ψ_m, and n allows the momentum field to respond to local stability changes throughout the model integration, and allows changes in

the momentum field to feed back into the local stability. It is remarkable that the model solution of Eq. (15) can reach a minimum constraint within 10 to 20 steps despite he local stability adjustments made through the computations described by Figure 6.

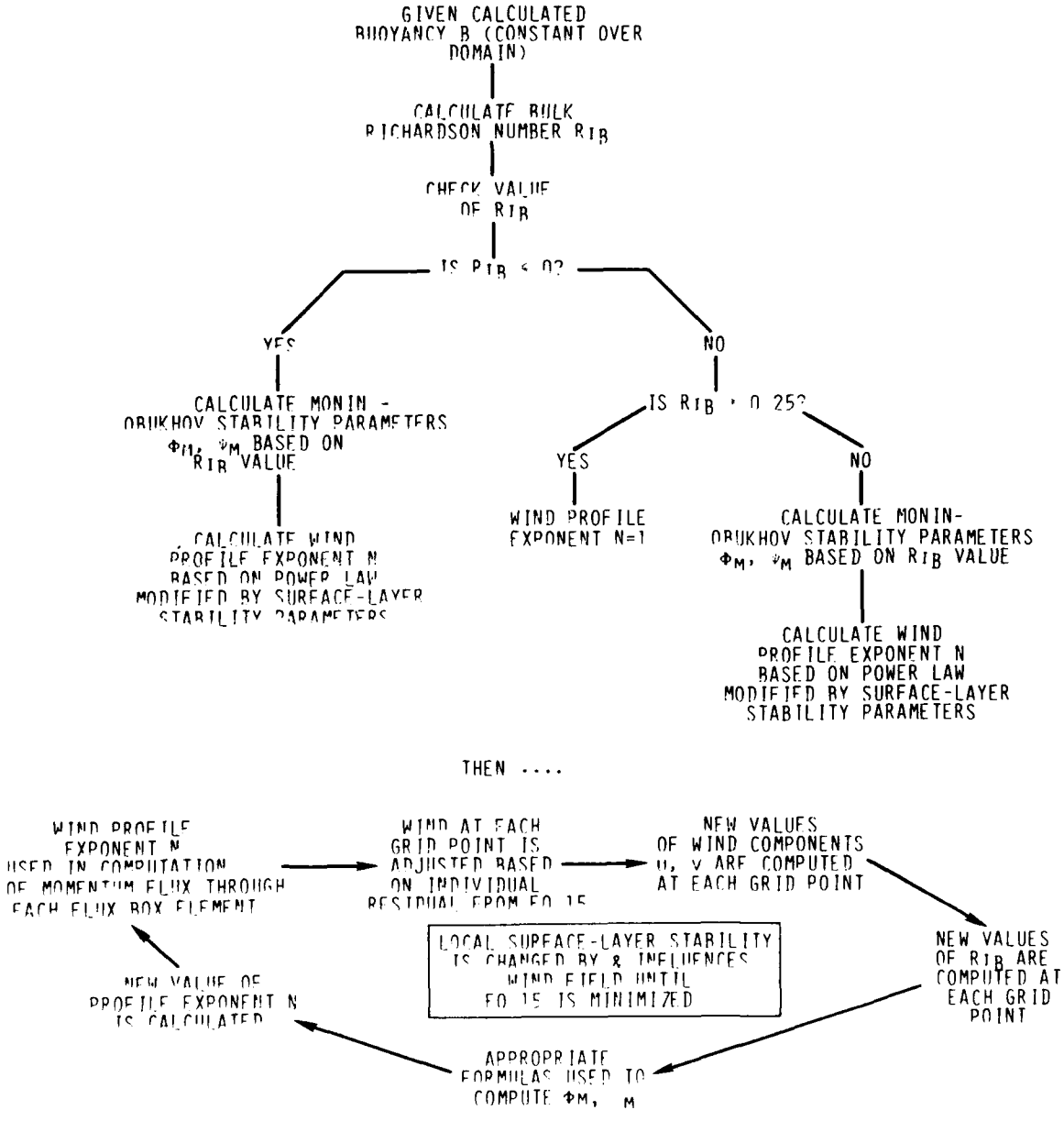

Figure 6. Flowchart Describing Calculation of Wind Profile Exponent n Based on Values of Buoyancy and Windspeed. Top flowchart shows calculation at individual grid point. Bottom flowchart shows how exponent calculation leads to changes in momentum flux, and changes in flux feedback to alter subsequent computations of n

Since the wind profile exponents computed in the model apply to conditions fairly close to the surface, use of these exponents to describe wind conditions at higher levels in the surface layer leads to overestimates of the wind speed. This occurs because the value of n in Eq. (21) is sensitive to choice of $\overline{Z}$. Field observations of wind profiles documented by Gringorten and Grantham[40] and many others show that the magnitude of the wind speed increases rapidly over the lowest 10 m (see Gringorten and Grantham's Tables 6.1, 6.3, and 6.5). The use of model wind profile exponents to determine windspeeds at higher levels is further discussed in Section 5 and Appendix A, and it will be shown that to calculate accurate surface layer wind profiles, the calculation height $\overline{Z}$ in Eq. (21) must be changed to represent the entire surface layer more accurately.

2.3 Appropriateness to Mesoscale Meteorological Analysis

One question that surely arises from the mathematical derivations presented in the previous two sections is: Do variational principles actually describe what the lower atmosphere is doing over complex terrain? The answer to this question lies in the approach taken in the formulation of the basic model equation [Eq. (15)]. Recall that the equation of motion can be derived through variational techniques by employing several simplifying assumptions such as incompressible and inviscid flow, or isentropic motion and inviscid flow. These approaches all retain the essential dynamics as embodied in the equation of motion. The windflow analysis is based on kinematic constraints, and represents a kinematic analysis of steady-state conditions under which the momentum advection and buoyancy force approximately balance under the constraints of topography (through the terrain-following coordinates) and mass conservation (through the incompressibility assumption). Therefore, Eq. (15) essentially describes a solution of atmospheric flow and does not attempt to describe the dynamic processes that lead to the solution. In many ways, the model solution expressed by Eq. (15) is similar to that obtained by running a PE model through some period of time until the model reaches a steady-state solution. Several modeling studies of slope flows have attempted this, and reveal that it may be easier to attain steady-state conditions under stable nocturnal conditions than under unstable conditions. During the night, a balance can occur along slopes between local cooling due to radiational and turbulent effects, and advective warming due to developing stratification (McNider and Pielke[41]). Even so, surges

40. Gringorten, I.I., and Grantham, D.D. (1983) Winds as a Function of Height, in Winds: Chapter 6, 1983 Revision, Handbook of Geophysics and Space Environments, AFGL-TR-83-0080, AD A132018.

41. McNider, R.T., and Pielke, R.A. (1984) Numerical simulation of slope and mountain flows, J. Climate and Appl. Meterol. 23:1441-1453.

in downslope flow intensity can occur, producing local accelerations in the flow (see the analytical study of McNider[42]). During the daytime hours, other physical processes such as horizontal diffusion of momentum by turbulent eddies can account for accelerations in the momentum field that persist for several hours before reaching a steady state (Banta[43]).

Several modeling studies have attempted to simulate flows over complex terrain using variational techniques. Most of these models fall into the so-called mass conservation type, since they relay on the continuity equation in one form or another for their analysis. An early attempt at this type of model was made by Anderson,[44] who generated terrain-induced wind fields using both the continuity equation (assuming incompressible flow), and a Poisson equation to represent thermal effects such as the urban heat island and topographic maxima or minima. This analysis was used for generating regional windflow climatologies for air pollution applications. Dickerson[45] developed a two-dimensional mass-consistent analysis based on a variational least squares technique first proposed by Sasaki,[26, 27] Dickerson's analysis sought to minimize the "error" between the observations of velocity flux components and height of the inversion base, and the adjusted values of these variables, weighted by appropriate factors based on the error variance of the observed field. A three-dimensional version of this model was also developed and documented by Sherman.[46] Other variational analysis models were proposed by Fox et al[47] and Goodin et al,[48] for windflow modeling problems, and also followed Sasaki's technique.

All of the above-mentioned modeling studies attempted to produce kinematically-constrained windflow analyses by assuming some type of steady-state condition

---

42. McNider, R.T. (1982) A note on velocity fluctuations in drainage flows, J. Atmos. Sci. 39:1658-1660.

43. Banta, R.M. (1986) Daytime boundary-layer evolution over mountainous terrain. Part II: Numerical studies of upslope flow duration, Mon. Wea. Rev. 114:1112-1130.

44. Anderson, G.E. (1971) Mesoscale influences on windfield, J. Appl. Meteorol. 10:377-386.

45. Dickerson, M.H. (1978) MASCON - A mass-consistent atmospheric flux model for regions with complex terrain, J. Appl. Meteorol. 17:241-253.

46. Sherman, C.A. (1978) A mass-consistent model for wind fields over complex terrain, J. Appl. Meteorol. 17:312-319.

47. Fox, D.G., Fosberg, M.A., Marlatt, W.E., and Reeser, W. (1976) Analysis of mountain air quality, Proc. of Third Symposium on Atmospheric Turbulence, Diffusion, and Air Quality, Am. Meteorol. Soc., Boston, Mass., pp. 470-475.

48. Goodin, W.R., McRae, G.J., and Seinfeld, J.H. (1980) An objective analysis technique for constructing three-dimensional urban-scale windfields, J. Appl. Meteorol. 19:98-108.

coupled with an appropriate condition such as incompressibility or mass-consistent flow. The advantages of these models are outlined below:

(1) Simplicity of physics,
(2) Computational efficiency (they can be run on smaller machines than PE models),
(3) High horizontal and vertical resolution over small regions,
(4) Inclusion of some physical processes (though kinematic in nature), thus superior to objective analyses, and
(5) Applicability to data-sparse areas (related to No. 4).

There are obvious disadvantages to these types of models. Some of them are listed here, and are further described throughout this report:

(1) Limited applicability to only certain meteorological situations, such as topographically-forced flows,
(2) Non-predictive nature,
(3) Emphasis on analysis of only one type of variable (usually winds),
(4) Difficulties in determining appropriate means of initialization and data input, and
(5) Limited physical parameterizations.

3. HARDWARE REQUIREMENTS AND MODELING SYSTEM SOFTWARE

This section describes the different computers on which we run the windflow modeling system. We also outline the computer architecture for the windflow model and the two plotting programs used to display the output. Complete program and subroutine descriptions are included, along with a flowchart of the model program.

3.1 Hardware

The windflow model runs on the Zenith 100 (Z-100) and Zenith 248 (Z-248) microcomputers, and on the Control Data Corporation Cyber 860 main frame computer.

The Z-100 on which most of the prototype development was done is a 16-bit desktop machine with 448 K random access memory (RAM), an added co-processor ("math chip") that speeds up arithmetic operations by about 10 times, dual diskette drives, and a high-resolution printer. Screen graphics produced by the model peripheral routines included windflow over the terrain and wind profiles. These were output to the 12-in. diagonal monochrome monitor capable of handling 640 × 225 addressable points and 25 printable lines of 80 columns each.

The Z-100 available at Ft. Devens did not have a math chip. Run time for a 15 × 15 array (200-m horizontal grid spacing) on this Z-100 varied from 12 to 20 min, depending upon the atmospheric stability conditions.

The AFGL Cyber 860 mainframe computer was used during early model development because of its superior size and compilation speed. The Cyber is a 60-bit large-scale machine that operates on a 24-hr schedule. As a result, many model runs were submitted simultaneously for overnight execution during the development and debug stages of the modeling effort. The Cyber computer was also used for developing the terrain data base files from the terrain data tapes. These files were then transferred to floppy disks for use on the Z-100 and Z-248.

During model development, AFGL acquired a Z-248 microcomputer. The Z-248 is IBM-compatible, about ten times faster than the Z-100 (with the math chip), has expansion memory to 3200K RAM with 20 megabyte hard disk storage, a 360K diskette drive, and superior graphics capabilities.

3.2 Software

The software for the windflow model was coded in Zenith Microsoft Fortran 77. The graphics utilities were written in Microsoft Z-Basic.

3.2.1 WINDFLOW MODEL

The main program MODEL calls three major modules INPUTD, WFMD and FLOUTD. INPUTD calls six subroutines in the process of setting up a particular model run. These input such variables as terrain heights for the selected domain, date and time, wind speed and direction, temperature, and cloud cover. Buoyancy and stability class are then calculated. WFMD is the windflow computational module, calling five subroutines to produce a high resolution, two-dimensional analysis of surface winds. FLOUTD creates three output files that contain the wind component arrays (u and v) for the domain, the power-law wind profile exponents, and the model input parameters.

The model provides space for a terrain array size up to 75 × 75 elements (44 × 69 on the Z-100). The model requires a minimum core of about 448K to be run. The size is located in a PARAMETER statement in an "INCLUDE" file and can be altered easily. All subroutines access common variables made available through five "INCLUDE" files provided at compilation time. A list of these files follows:

(1) WINDZZ.INC—contains the allocation for array size for the model, used for the terrain heights, surface roughness, wind components, wind exponent, and buoyancy arrays. In addition, space is allocated for the computed terrain slopes, and common variables for the windflow model are stated.

(2) WINDBZ.INC—provides space for the wind speed, direction and surface temperature.

(3) DIFUSAA.INC—provides space for constants used in calculating buoyancy.

(4) WINDAZ.INC—provides common storage for the terrain input file name.

(5) DATEZ.INC—provides space for date/time information.

The routines called by the modules INPUTD, WFMD, and FLOUTD are described below. A complete flowchart of the windflow model is displayed in Figure 7.

INPUTD executes all input subroutines. These are:

(1) GETTER—inputs domain terrain data array limits (horizontal and vertical), rid size, longitude and latitude, roughness indicator.
   - inputs terrain data
   - creates constant roughness array (50 cm over Ft. Devens in prototype)
   - sets calculation height for windflow at 32.8 ft (10 m) AGL
   - calculates terrain slopes
   - inputs date and time

(2) SOLAR—calculates solar radiation based on date, time, latitude and longitude.

(3) WINDIN—inputs wind direction in degrees and speed in knots and uses these to initialize wind component arrays (u and v, in m/s) at each gridpoint. Rotates components 45° to orient axes along direction of calculated terrain slopes.
   - inputs cloud cover in eights (use look-up table to adjust solar radiation computation for type of cloud cover)

(4) STAB3—calculates the stability parameter (between 0.5-6.0).

(5) TSRFIN—inputs surface temperature in °F and converts it to Kelvin.

(6) BUOYIN—calculates the buoyancy at each grid point using temperature and stability parameter.
   - displays buoyancy and stability parameter and returns to main program.

WFMD sets the maximum number of relaxation steps at 60. It displays the array size for the windflow calculation and allows choice of smaller array window. It also displays the current relaxation step and tests to see if constraint has reached minimum. This module calls five subroutines.

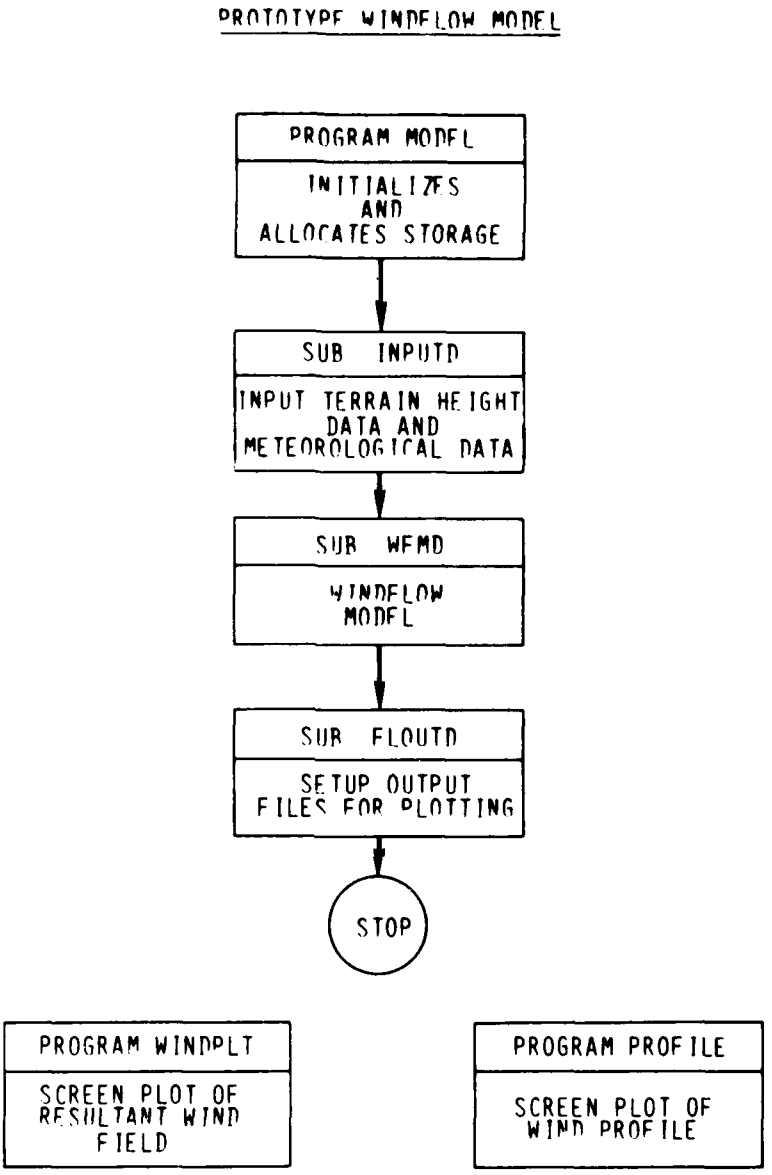

Figure 7. Flow Chart of Windflow Model Program and Peripheral Software. Also shown are flowcharts for the main modules INPUTD and WFMD

(1) RELAX—calls routines to calculate local contributions to the acceleration residual.

- accumulates residuals
- calculates partial derivatives of residuals with respect to wind components at each gridpoint
- applies incremental adjustments to wind field

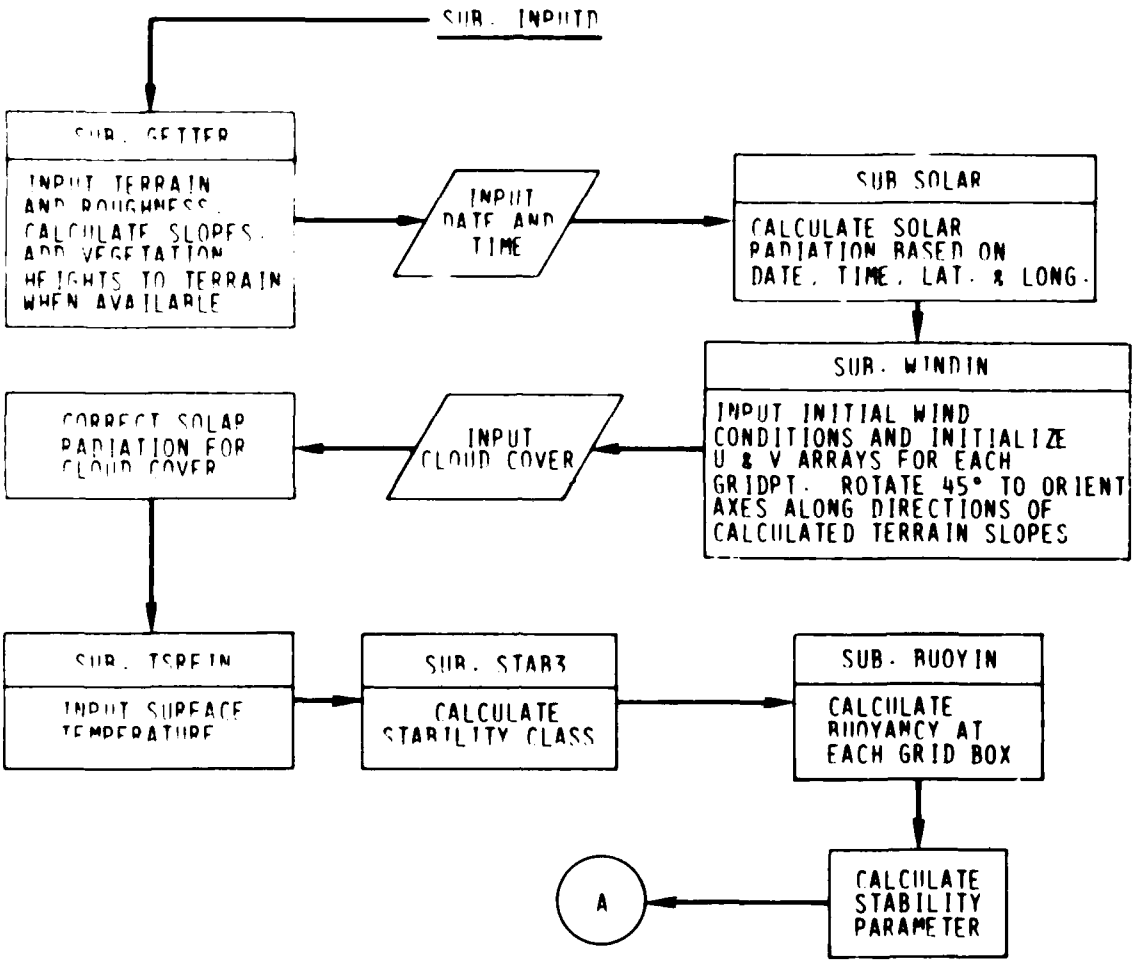

Figure 7. Flow Chart of Windflow Model Program and Peripheral Software. Also shown are flowcharts for the main modules INPUTD and WFMD (Contd)

(2) WINEXP—computes the wind profile exponent at each gridpoint.

(3) SETBOX—selects the parameters for the local residual.

(4) RESLOC—calculates the integral of the residual squared over a local volume element (flux box).

(5) OUTPUT—rerotates calculated wind components 45° to return to original Cartesian coordinates.

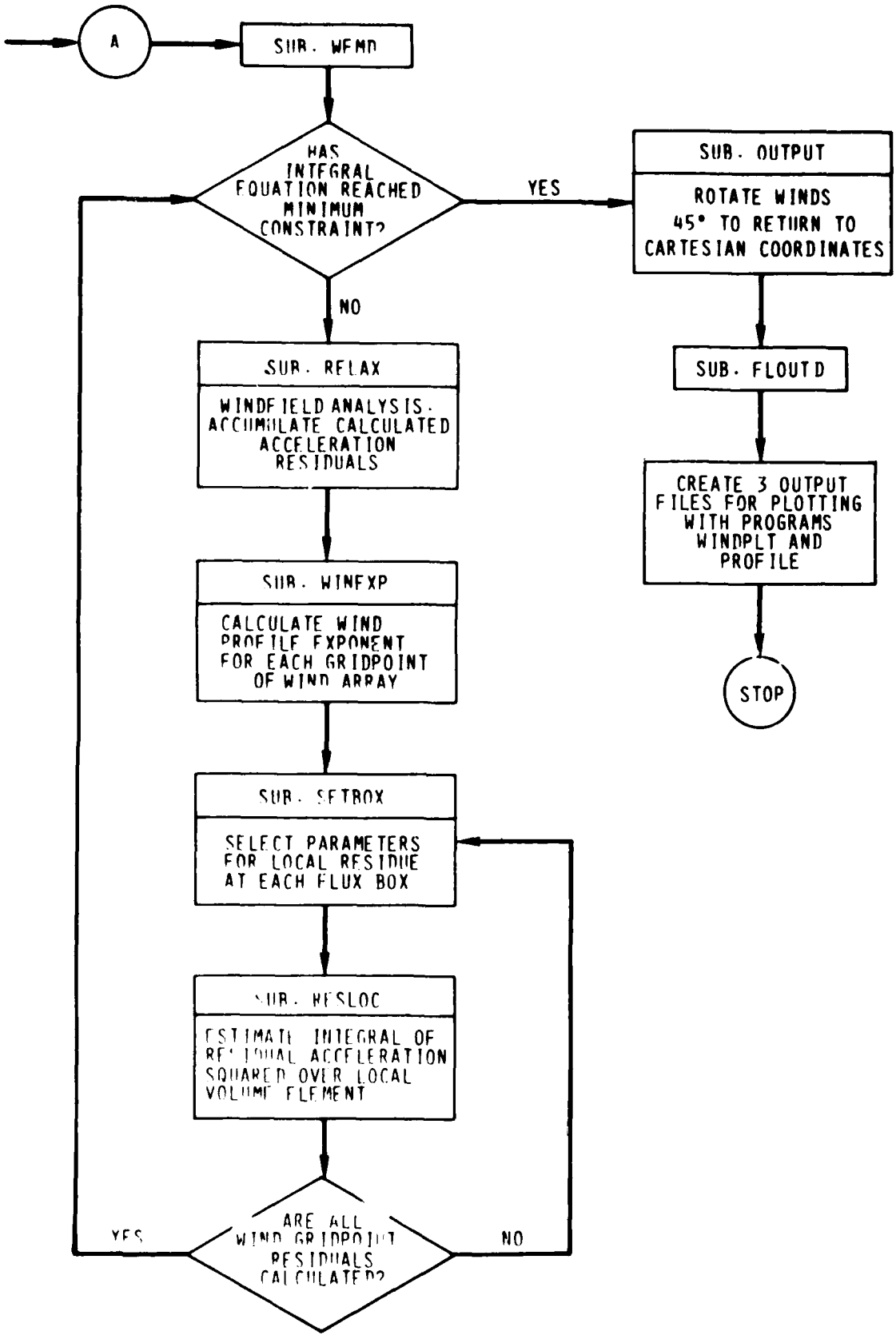

Figure 7. Flow Chart of Windflow Model Program and Peripheral Software. Also shown are flowcharts for the main modules INPUTD and WFMD. (Contd)

FLOUTD creates three formatted output files to be used by the utility plotting routines to display output on the screen.

(1) WIND.OUT—contains u, v, component arrays for a size m x (west-east) by m y (south-north).

(2) WEX.OUT—contains wind profile exponent array for m x by m y size.

(3) MODIN.OUT—contains model input and output parameters. These are model computation height, day, month, year, time, wind direction and speed, surface temperature, cloud cover, cloud type if cloud cover is 7/8 or 8/8, diagnosed stability parameter, and mean wind profile exponent over window.

3.2.2 HORIZONTAL WIND PLOT FOR SCREEN

This routine, called WINDPLT, displays the windfield over a selected window (the user can choose the array size for the display). The winds can be displayed either as arrows with length proportional to speed (in this option the program calculates the maximum windspeed encountered over the chosen display window and asks the user if he would like to use this value for the scale), or in conventional plot notation with barbs. The program displays the winds in kt, and also displays the date/time, mean direction and speed throughout the window, mean profile exponent, stability parameter, and model calculation height in feet. Depressing the space bar on the keyboard after the display is completed causes the program to ask if the user wants another plot or to end the program. There are two versions of this program; one for the Z-100 and another for the Z-248.

3.2.3 VERTICAL WINDSPEED PROFILE SCREEN PLOT

This routine, called PROFILE, displays a windspeed profile from 32.8 ft to 300 ft if the user selects the speed in kt option, or from 10 m to 100 m if the ms^{-1} option is selected. The user inputs the windspeed and exponent using either the model-generated values obtained from the horizontal wind plot, or user-selected values. As in the horizontal plot, hitting the keyboard space bar results in a choice of another plot or program termination. This program also exists in Z-100 and Z-248 versions.

4. A USER'S GUIDE TO THE WINDFLOW MODELING SYSTEM

The purpose of this chapter is to familiarize the user with the operation of the windflow model. Since a large group of potential model users may be operational forecasters with little training in boundary-layer meteorology, we have included Section 4.1 to give the forecaster an introduction to the dynamics of the

lower atmosphere. This introduction will serve as a basis for subsequent discussions of the model's formulation (Section 4.2) and rules for interpreting the output (Section 4.3) under varying atmospheric conditions. Becoming familiar with this section will make the interpretation of the results of the Ft. Devens field tests in Section 5 easier.

4.1 Introduction to the Dynamics of the Lower Atmosphere

This section is not intended to provide a comprehensive review of the dynamic meteorology of the lower atmosphere. Instead, it provides the necessary background for understanding how the windflow model operates, as well as the limitations it has. Material in this section is drawn primarily from Anthes et al[49] and Wyngaard.[50]

The windflow model produces a high-resolution analysis of surface winds as influenced by the stability of the lower atmosphere and the topography. To better understand the relationship described by the model, we begin with some definitions. The lower atmosphere is often referred to as the planetary boundary layer, or PBL. The PBL is defined as that layer of the atmosphere where the effects of the earth's surface are dominant. During the day, the PBL (typically 1-2 km deep) is influenced by turbulent mixing of momentum, heat, and moisture. This turbulent mixing occurs because the atmosphere is largely transparent to solar radiation and most of the sunlight heats the ground instead of the air. As the ground heats up during the day, it conducts heat both downward and upward. The upward conduction causes the air very close to the ground to heat up and expand, thus rising above cooler, denser air above it. Bubbles of heated air begin to rise while cooler air sinks to the ground and is heated by the ground. As these heated bubbles of air rise, they mix with air aloft and heat it. The rising and sinking bubbles are called convection currents, and they are the primary means by which turbulent mixing occurs in the daytime PBL. At night, the ground radiates heat away to space, and the air above the ground slowly cools by radiation too. The PBL becomes much shallower because turbulent mixing due to surface heating has ceased and a surface-based temperature inversion forms. If there is mixing at night, it is usually caused by strong winds (mechanical mixing). The depth of the PBL increases with windspeed and surface roughness.

---

49. Anthes, R.A., Panofsky, H.A., Cahir, J.J., and Rango, A. (1978) The Atmosphere (2nd Ed.), Merrill Publishing Co., Columbus, Ohio, pp. 128-131.

50. Wyngaard, J.C. (1985) Structure of the planetary boundary layer and implications for its modeling, J. Climate and Appl. Meteorol. 24:1131-1142.

Typical profiles of temperature for daytime and nighttime conditions are shown in Figure 8. Notice that the effect of strong winds is to alter the thermal structure through mechanical mixing so that the daytime and nighttime profiles become more similar.

The windflow model considers that portion of the PBL known as the surface layer. The surface layer is usually considered to be the lowest 10 percent of the PBL. It is a layer through which vertical transport (flux) of momentum, heat, and moisture can be considered constant. During the daytime the surface layer, like the PBL, is well-defined. The problems associated with defining the nighttime PBL also apply to the surface layer (this problem will be highlighted further in Section 4.3). The temperature profiles over the lowest 100 m in Figure 8 are typical of the surface layer. Notice that strong vertical temperature gradients can exist in the surface layer. The surface-layer stability is a measure of the magnitude of the vertical temperature gradient. Stability used in this context is not the same as the "static stability" used to describe conditions favorable for thunderstorm formation. There are three basic states of surface-layer stability based on the vertical temperature gradient. Unstable conditions (that usually appear during the day) occur when the vertical temperature gradient is less than -1°C 100 m^{-1}. Stable conditions (usually appearing at night) occur when the vertical temperature gradient is greater than -1°C 100 m^{-1}. Neutral conditions, that usually occur under cloudy and/or windy conditions, or at sunrise and sunset, correspond to a vertical temperature gradient equal to -1°C 100 m^{-1}. The -1°C 100 m^{-1} value is also known as the dry adiabatic lapse rate (the temperature lapse rate obtained by following the dry adiabats on a conventional Skew T-Log P diagram). It is important to understand these definitions concerning surface-layer stability since they are not normally resolved on conventional temperature-dewpoint soundings (for instance, an unstable layer on a sounding appears as a "superadiabatic" layer, which does not occur very often since the vertical resolution is not fine enough). For this reason, the model diagnoses stability based on the surface input information given to it by the user.

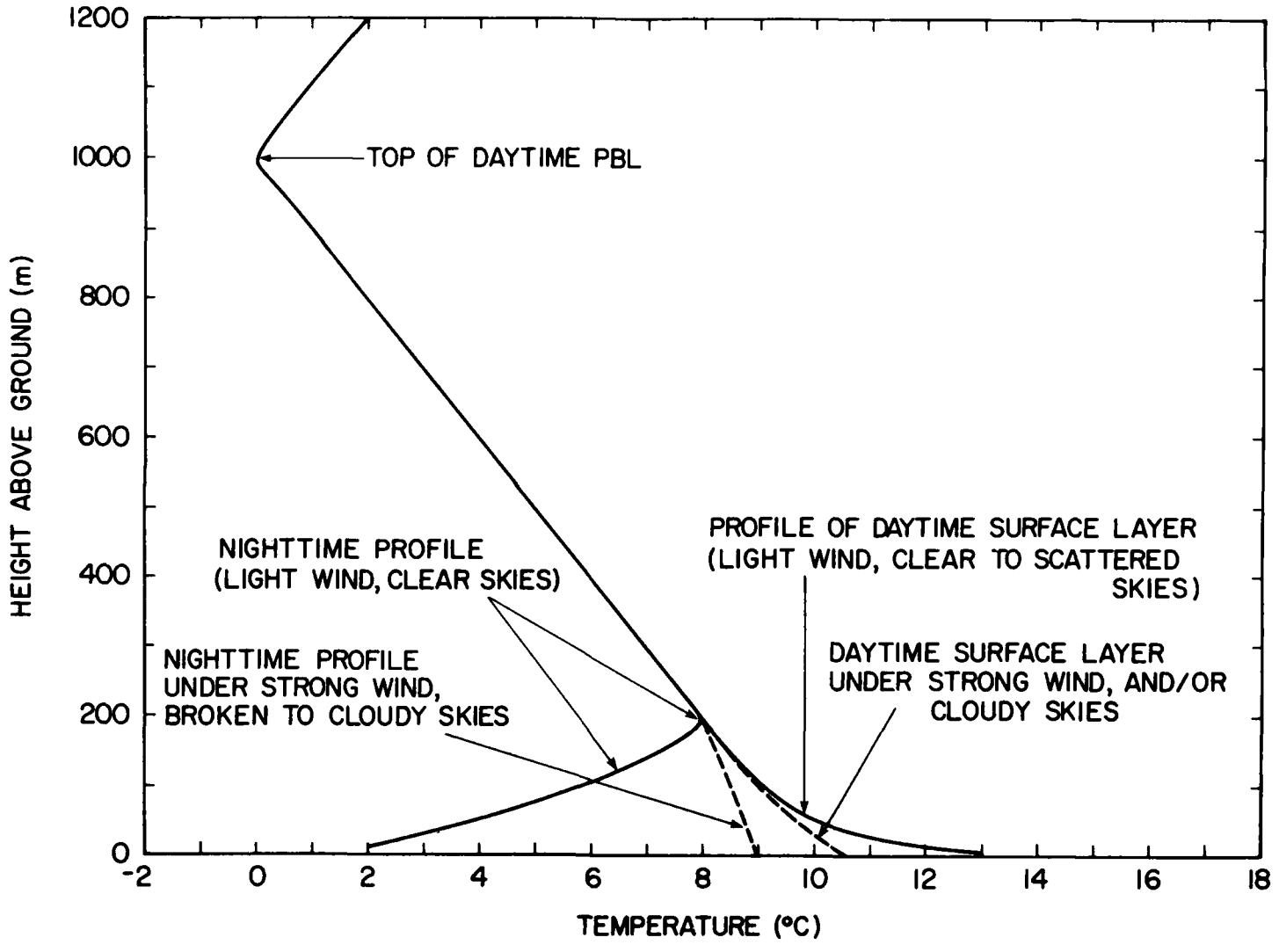

Figure 8. Profiles of PBL Temperature for Daytime and Nighttime Conditions, Under Light Wind, Clear Sky Conditions (solid lines) and Cloudy Skies/Strong Winds (dashed lines)

Typical surface-layer wind profiles for daytime and nighttime conditions are shown in Figure 9. During the daytime, windspeed increases with height to about 100 m and is approximately constant throughout the rest of the PBL. At night, the winds are typically light near the surface, but increase rapidly with height until the top of the nocturnal temperature inversion is reached. At this level, a wind maximum called a "nocturnal jet" is often encountered. Quite often, the nocturnal jet is referred to as a "low-level jet." These two phenomena are closely related, but the low-level jet is a broader category that includes those jets whose formation can be explained by their interactions with upper-level jets (Uccellini and Johnson[51]) as well as those strong low-level jets associated with nocturnal thunderstorm activity over the Great Plains (Means;[52] Lettau;[53] Blackadar;[54] Pitchford and London;[55] Bonner[56] and many others). The nocturnal jet, by contrast, may not be that strong, and is usually associated with the formation of the nocturnal temperature inversion. It should be noted that under neutral conditions both the wind and temperature profiles tend to be more uniform with height due to the effects of mechanical mixing. Now that we have discussed the PBL and surface layer, we can summarize the wind and temperature characteristics for each of the three stability classes. This is done in Table 2.

We now discuss the effects of topography on the surface windflow. In general, the profile relationships outlined in Table 2 are still valid over sloping terrain, but with some important additional effects.

---

51. Uccellini, L. W., and Johnson, D. R. (1979) The coupling of upper and lower tropospheric jet streaks and implications for the development of severe convective storms, Mon. Wea. Rev. 107:682-703.

52. Means, L. L. (1944) The Nocturnal Maximum of Thunderstorms in the Mid-western States, Miscellaneous Report No. 16, University of Chicago.

53. Lettau, H. H. (1954) Graphs and Illustrations of Diverse Atmospheric States and Processes Observed During the Seventh Test Period of the Great Plains Turbulence Field Program, Occasional Report No. 1, Atmospheric Analysis Laboratory, Air Force Cambridge Research Center.

54. Blackadar, A. K. (1957) Boundary-layer wind maxima and their significance for the growth of nocturnal inversions, Bull. Am. Meteorol. Soc. 38:283-290.

55. Pitchford, K. L., and London, J. (1962) The low-level jet as related to nocturnal thunderstorms over the midwest United States, J. Appl. Meteorol. 1:43-47.

56. Bonner, W. D. (1968) Climatology of the low-level jet, Mon. Wea. Rev. 96:833-850.

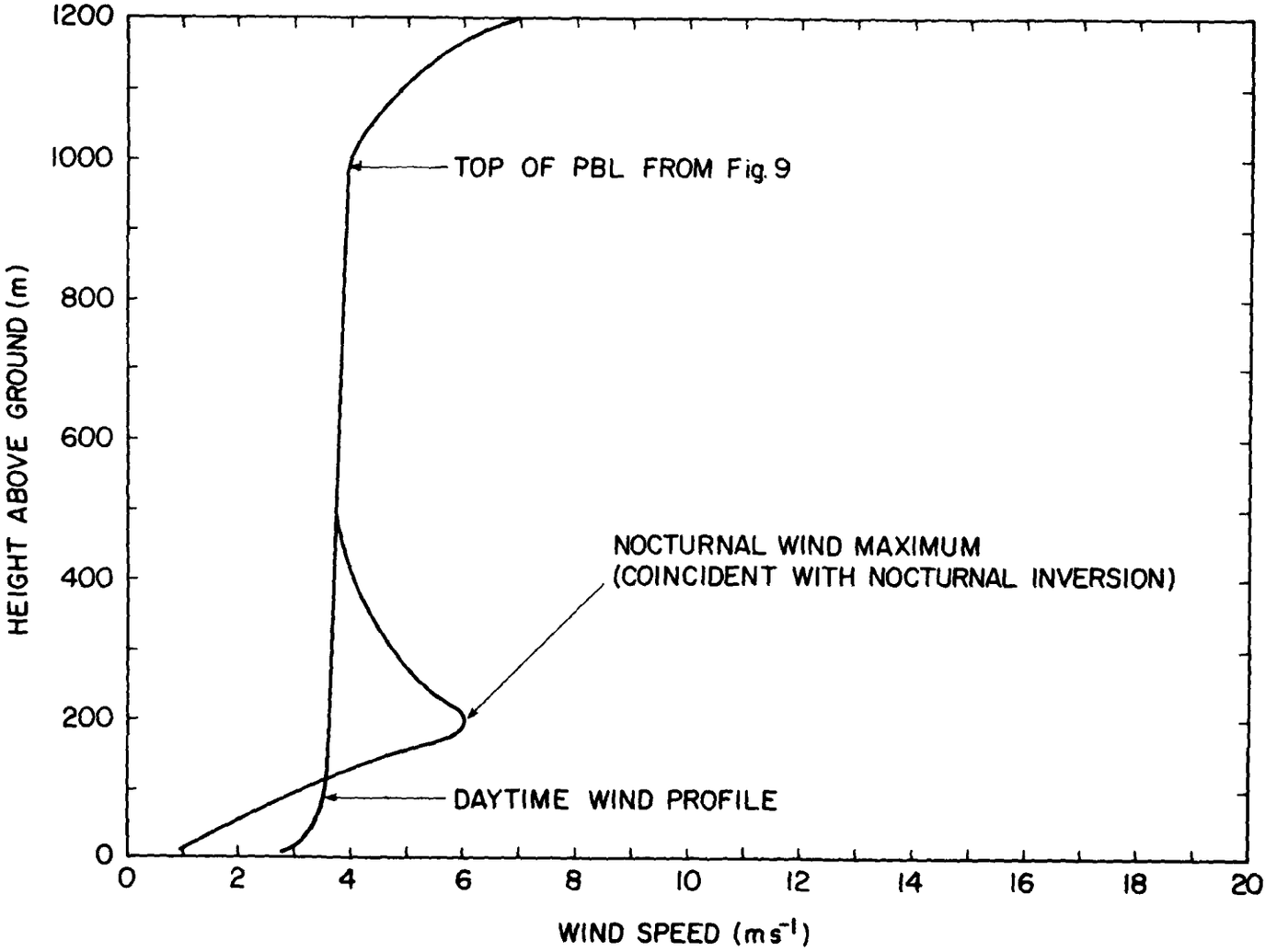

Figure 9. Profiles of PBL Windspeeds for Daytime and Nighttime Conditions

Table 2. Wind and Temperature Characteristics Under Different Stability Conditions

Surface-Layer Stability	Most Common Meteorological Conditions	Wind Profile Characteristics	Temperature Profile Characteristics
Unstable	Daytime*, Light Winds, Clear to Scattered Skies	Increase w/height in lowest 50-100 m, approximately uniform to top of PBL	Strong decrease w/height in lowest 50-100 m, then dry adiabatic ($-1°C\ 100\ m^{-1}$) above to inversion at top of PBL
Stable	Nighttime**, Light Winds, Clear to Scattered Skies	Near calm at surface, strong increase w/height above surface to top of temperature inversion, then decrease above to daytime top of PBL	Increase or isothermal w/height to a level somewhere below daytime top of PBL, then dry adiabatic above to inversion at daytime top of PBL
Neutral	Sunrise, Sunset, Strong Winds and/or Cloudy Conditions	Increase w/height in lowest 50-100 m, then uniform above to top of PBL (daytime) or to stable layer (nighttime)	Approximate dry adiabatic w/height ($-1°C\ 100\ m^{-1}$) to top of PBL (daytime) or to stable layer (nighttime)

*An unstable layer can also be found near the surface in urban areas at night (known as urban heat island effect).

**A stable layer near the surface can sometimes be found during the day in winter at high-latitude locations, or at mid-latitude locations with either a snow cover or arctic high conditions.

During the day, the ground is heated, but the heating is stronger over sloping terrain facing the sun than over level ground due to a more direct solar angle. The slope surface heating induces a horizontal temperature gradient between the air close to the slope and the free atmosphere at the same elevation (see Figure 10). These temperature differences induce differences in pressure, so a pressure gradient force from the free air to the slope is generated. Meanwhile, an unstable vertical temperature gradient exists above the sloping ground and produces an

upward buoyancy force. These two forces cause the air to accelerate horizontally toward the slope and vertically above the slope, and the presence of the terrain serves to direct this accelerated flow "upslope." At night, the pressure gradient force is directed away from the slope (since the air temperature above the sloping ground is cooler than the free air at the same level), and the stable lapse rate above the sloping ground causes a downward buoyancy force. The combination of these two forces in the presence of the terrain causes a "downslope" wind to appear.

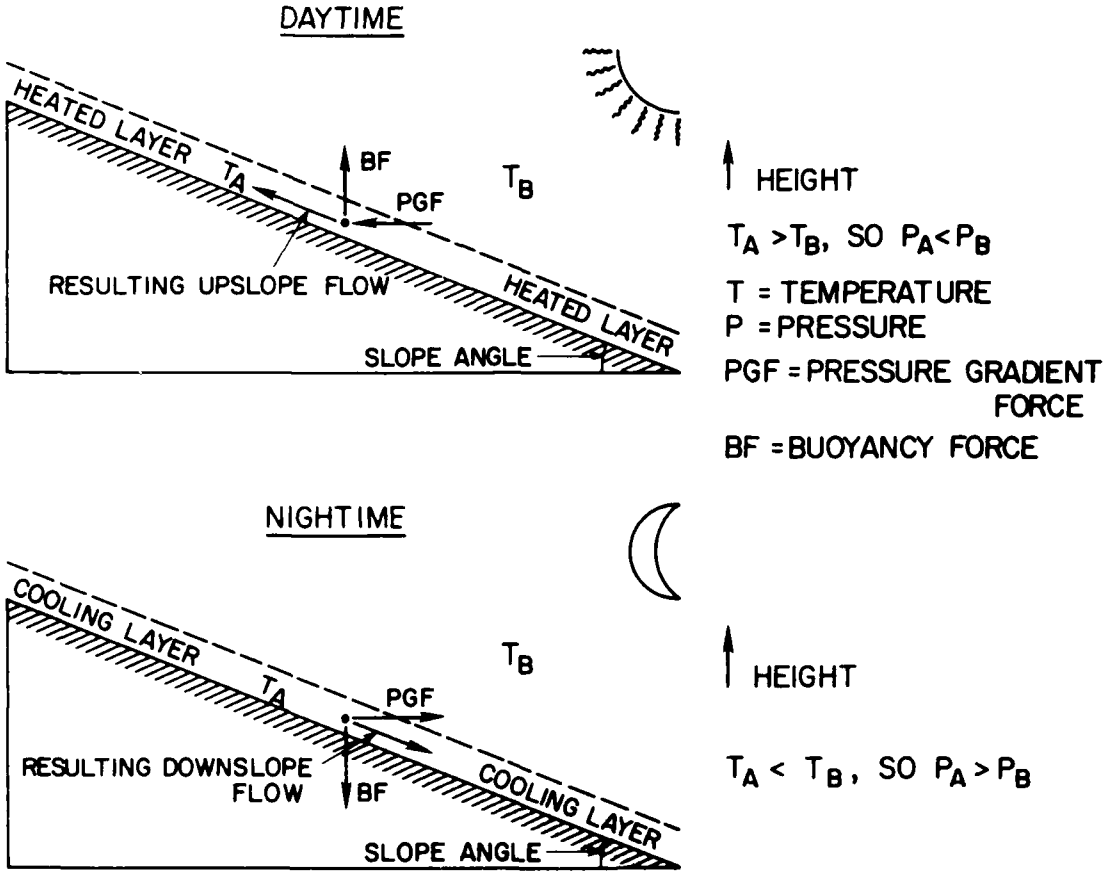

Figure 10. Diagrams Showing Slope Heating (top) and Cooling (bottom) Effects on Formation of Slope Winds (after Atkinson[30])

The slope flows described above are also influenced by the strength of the prevailing winds as well as the presence of clouds. Under strong winds and/or cloudy conditions, the slope heating effects are weakened and the flows along the slopes are more aerodynamic (that is, influenced by the forces resulting from the wind-flow interaction with the terrain obstruction).

4.2 Model Formulation and Physical Assumptions

The windflow model runs on a grid system that produces calculations of wind speed and direction, taking the slope of the surrounding terrain into account. The model begins with a uniform windfield, and makes small adjustments at each grid point over the model domain. This adjustment is called a relaxation step. After a number of relaxation steps, the model has integrated the effects of ambient flow, stability, and topography to reach a solution and the model run ends. The model may take a different number of steps to reach a solution depending upon the meteorological situations. At the end of this section, we describe a way for the user to tell approximately how many steps a model run will take for different cases.

The easiest way to describe the model formulation is to outline a sample session with the model (see Figure 11). The Z-100 and Z-248 versions are essentially identical, so the session described here is applicable to either machine. The model first reads in digital terrain elevation data for the area of interest, noting the latitude and longitude of the location for calculating solar elevation angles and solar radiation. The model also reads in the surface roughness, a parameter that describes the character of the land surface. The model calculation height is set equal to 10 m above ground level (AGL) because the flow at this level is strongly influenced by the land surface features. Next, the date and time (in GMT) are input for the model to complete its solar radiation computation. The wind direction and speed are entered next and the model sets up the uniform initial windfield. If light and variable or calm winds are reported or forecast, use either the predominant observed direction or make multiple runs using different directions (the default windspeed in the model is 1 kt). The next piece of information is the cloud cover in eighths. This input presents a problem when cloud decks exist at different levels. Table 3 describes the cloud input using observations and military terminal aerodrome forecast (TAFs). For 7/8 and 8/8 cloud cover (overcast conditions), the model asks you to choose from eight different cloud types, ranging from cirrus to fog. Table 4 shows the guidelines for input of cloud-type based on either observations or TAFs. Notice that for broken cloud decks with an overcast layer above, the dominant cloud type corresponds to the deck at ceiling level, not overcast level. This is because the model considers the effects of all cloud layers on the amount of solar radiation reaching the surface. At night, the downward heat flux reaching the surface is more affected by the presence of low clouds than by upper-level cloud layers. The model finally asks for surface temperature, and then displays the stability parameter corresponding to the input data given to it by the user. In general, a stability parameter below 3.3 corresponds to unstable conditions, from 3.3 to 3.7 is neutral, and above 3.7 is stable. One has the option of running the

```
D:\JOAN\ MODEL CR
TERRAIN DATA INPUT FROM TER. DAT
.....

LOWER LEFT CORNER OF DOMAIN

LONGITUDE  DEG    71
           MIN    36
           SEC     0
LATITUDE   DEG    42
           MIN    34
           SEC     0

A CONSTANT ROUGHNESS IS USED
HEIGHT OF WIND INPUT

32.8 FEET  DEFAULT VALUE
DATE INPUT
.....
---------->DAY
  ---------->MONTH (1ST 3 LETTERS)
    -------->YEAR

V    V    V
12 MAR 1984   <==  EXAMPLE


V    V    V    <== PLEASE ENTER DATE
8 JAN 1987 CR
TIME INPUT ZULU
.....
---------->HOUR

  ------->MINUTE

V  V
13 05    <==  EXAMPLE

V  V     <==  PLEASE ENTER TIME IN ZULU
16 00 CR
---------->WIND DIRECTION IN DEGREES

  ----->SPEED IN KNOTS

V  V     <==  ENTER VALUES
330 15 CR
CALCULATION OF START WIND ARRAY

CLOUD INPUT
.....

PLEASE ENTER CLOUD COVER IN EIGHTS
0 CR
SURFACE TEMPERATURE INPUT
.....
---------->SURFACE TEMPERATURE
           IN DEGREE FAHRENHEIT

V    <== ENTER VALUE

32 CR

CORRESPONDING BUOYANCY IS = -.004
STABILITY PARAMETER
.....
CALCULATED USING SOLAR INPUT      3.5
THE DEFAULT WINDOW FOR
THE WIND FLOW MODEL IS :

I  WEST    :    1
I  EAST    :   43
J  SOUTH   :    1
J  NORTH   :   68

HIT RETURN FOR THE DEFAULT VALUES OR ENTER<C>
TO CHANGE THEM
C CR
---------->I WEST
  ---------->I EAST
    ---------->J SOUTH
      -------->J NORTH

V .V .V .V
8.22.15.29  CR
THE AFGL WIND FLOW MODEL IS RUNNING

PLEASE WAIT

THIS IS RELAXATION STEP 1
THE AFGL WIND FLOW MODEL IS RUNNING

PLEASE WAIT

THIS IS RELAXATION STEP 2
THE AFGL WIND FLOW MODEL IS RUNNING

PLEASE WAIT

THIS IS RELAXATION STEP 3
Stop - Program terminated.
```

Figure 11. A Sample Interactive Session Using Surface Observation as Input to Windflow Model. Input by user is indicated by an "I" in left-hand column with a "CR" after input data to indicate carriage return on keyboard

Table 3. Cloud Information Input

Using Observations:	
Observed Sky Condition	Cover Input to Model
Clear	0
Scattered (one deck)	1, 2
Scattered (two decks)	3
Scattered (more than two decks, no ceiling	4
Broken (ceiling above 10,000 ft, no overcast deck)	5
Broken (ceiling below 10,000 ft, no overcast deck)	6
Broken with overcast above, or Fog with visibility ≧ 1 mi, < 3 mi*	7
Overcast, or Fog with visibility below 1 mi*	8

Using TAFs:

Input cloud cover in eights from sky condition on TAF using guidelines above for multiple cloud decks.

*For situations with both clouds and fog, run the model twice, using the cloud condition and then using the fog condition.

model for the entire domain or over a window of that domain. The example in Figure 11 shows that a 43 × 68 array has been specified for Ft. Devens, Massachusetts, that translates into 2924 grid points at which model calculations are performed. A window of the domain has been chosen that corresponds to the drop zone at Ft. Devens. This window is a 15 × 15 array, or 225 grid points.

The number of steps the model will take to reach a final solution is primarily dependent upon two factors. The first factor is the stability parameter, and the second one is the ruggedness of the terrain. The model will converge to a solution faster if the stability parameter is close to neutral (between 3.3 and 3.7). As the stability parameter increases beyond 3.7, or decreases below 3.3, the model run time will increase as well. For example, over Ft. Devens, the model took about 18 to 20 steps to reach a solution for very stable cases (stability parameter = 6.0, the highest value), and about 23 to 34 steps for unstable cases. For neutral cases,

Table 4. Cloud Type* Input (7/8 or 8/8 Cloud Cover)

Observations:
The predominant cloud deck should be the one at which the ceiling is located (that is, 35 BKN 80 OVC should be treated as 7/8 cloud cover with predominant cloud type Sc).
TAFs:
Same as observations (that is, 2 St 008 5 Sc 035 7 AS 100 CIG 035 should be treated as 7/8 cloud cover with predominant cloud type Sc)

*See Appendix B for definitions of the cloud type abbreviations.

the model usually runs in a minimum of two steps. Over more rugged terrain such as Vandenberg AFB, California, the model run time increases for stabilities just below 3.3 and above 3.7, but remains about the same for the extreme cases. This relationship is described in Figure 12.

4.3 Rules-of-Thumb for Interpreting Model Output

In this section, we document those situations that the windflow model handles well, as well as those cases in which the model output may not be as reliable. The windflow model output can be displayed in two ways. The first is by a horizontal plot of the winds at 10-m AGL. It is advisable to overlay a terrain map with geographic features on the horizontal wind plot in order to see the terrain-induced wind features in graphic detail. The second is a vertical windspeed profile over the lowest 100 m (about 300 ft), described in Section 3.3. This wind profile output warrants separate discussion that appears in Section 4.3.2.

4.3.1 INTERPRETATION OF HORIZONTAL WIND PLOTS

In general, the windflow model produces the best results when it is initialized with input information that is *representative* of the area being analyzed. The model domain is usually on the order of about 10 × 10 km; so a single observation is somewhat representative. However, we should give you a few pointers to ensure that this is true. First, a good knowledge of the microclimate is essential before running the model. Consider such factors as proximity of water bodies such as

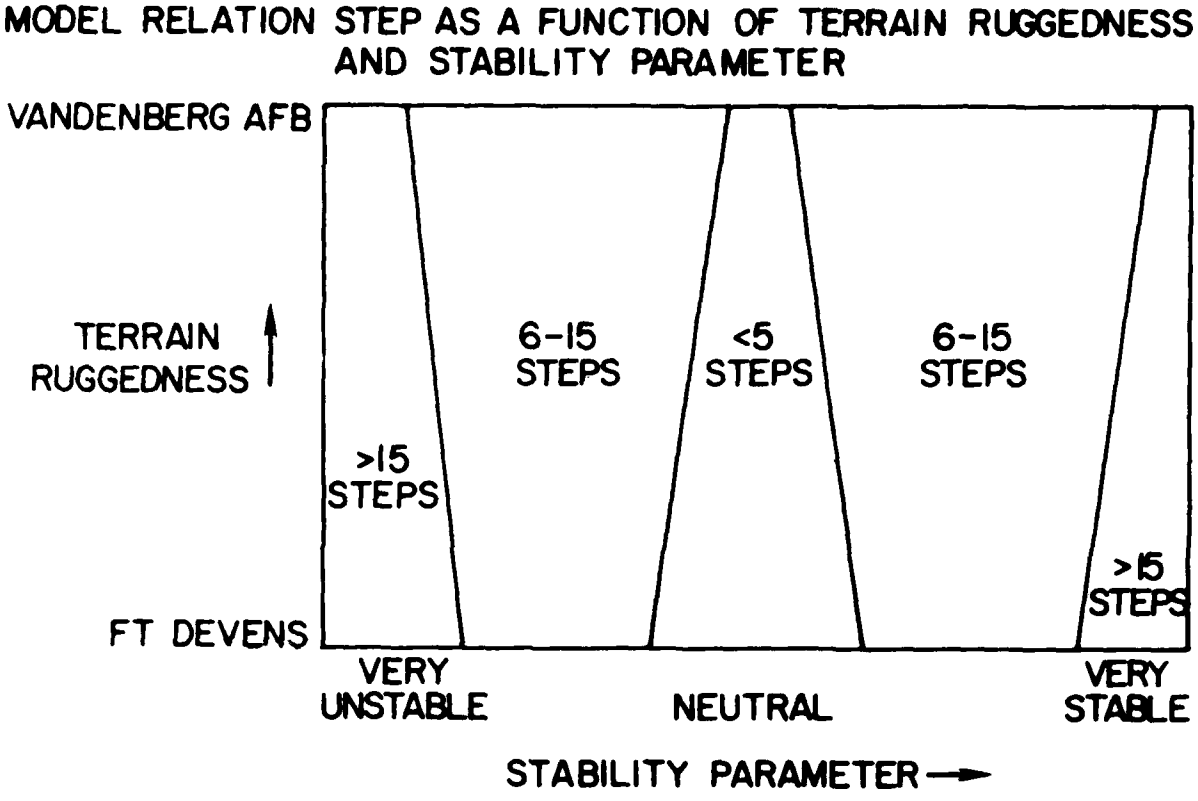

Figure 12. Diagram Illustrating Approximate Number of Steps the Model Takes to Reach a Solution as a Function of Stability Parameter and Terrain Ruggedness. This diagram should be used as a guide only; actual results could be different

large lakes or oceans that could produce local circulations such as sea and land breezes. These local phenomena may produce different stabilities in different locations (for example, neutral conditions at the shoreline and unstable inland), and using the observed wind from one locale (such as the beach) may not be representative of the entire area you are interested in. Multiple model runs should be made with different type of inputs that cover the different possibilities for a given time. Using the coastal example, try using input conditions (such as neutral for the coastline, then unstable for the interior), that will yield different model solutions over the domain, and compare the results. If you are unsure of the representativeness of the local wind observation, compare it against a derived value from the local surface analysis, such as a geostrophic or gradient wind. Make model runs using these different wind inputs and compare the results. For forecast applications, the output from a model-output statistics package can give you a representative "observation" to use in the model run. Compare this output with that using the TAF as input.

Having established the different ways in which to arrive at a representative input for the model, we should discuss how to interpret the output. If multiple model runs are made for a given situation, the user must choose which output is best. One way to do this is to have already prepared a model wind climatology for different synoptic patterns at different times of the day, times of the year, and so on. After running the model for a particular forecast time, compare the output with that from the climatological simulation for that type of synoptic flow regime. This comparison should give you a first guess at how representative the model run may be for the particular date and time of interest.

There are two other factors necessary to interpret the model output. One factor is your knowledge of the local climate, as previously discussed with regard to the representativeness of the input observation. The second factor is a knowledge of the inherent strengths and weaknesses of the windflow model. Knowledge of model strengths and weaknesses is important regardless of the location and situation, and potential users should become very familiar with this information before using the model. Table 5 lists the model strengths and weaknesses, and we now discuss these in detail.

Table 5. Model Strengths and Weaknesses

Strength
– Cold-air drainage flows
– Daytime upslope flows*
– Flow under homogeneous wind or stability conditions
– Effects of vegetation on the flow (light winds, stable or unstable conditions)
Weaknesses
– Flows under nonhomogeneous wind and stability conditions
– Flows over flat terrain areas
– Light wind cases when no vegetation data are available
– Model cannot be applied over very mountainous regions (see text)

*There is a tendency for the model to exaggerate upslope flow conditions over gentle topography under very unstable (for example, stability parameters 0.5 - 1.0) conditions

The model can simulate terrain-induced flows such as cold-air drainage and upslope flows, and integrates the effects of stronger winds into the solution. Strong flows tend to show little terrain influence over gentle topography, but some influence almost always remains over rugged terrain. If stability conditions are fairly homogeneous over the area, the model results can be relied upon. If digital vegetation height data are available for a location, the model is especially capable of integrating the effects of vegetative cover into the flow patterns under light winds (see Lanicci[23]). If the model is used to support NBC operations (see Section 1.1), we strongly recommend the acquisition of vegetation data for addition to the terrain information already used by the model.

The model has several weaknesses that must be considered when interpreting the output. The first of these weaknesses pertains to the presence of non-homogeneous stability and wind conditions over an area. Several examples are given below:

(1) Coastal regions (especially mountainous areas like Vandenberg)—particularly around sunrise and sunset, when coastline stability may be neutral or slightly stable, while the interior remains unstable; sea breezes with weak gradient-level winds, or when a sea-breeze "front" produces mesoscale convergence and localized clouds or precipitation.

(2) Very mountainous regions (areas like the Continental Divide of North America)—In these locations, the high terrain is under a vastly different flow regime than the lowlands are, so a three-dimensional model would be more appropriate.

The model has problems over flat terrain (although most regions of application will have few flat areas in them) because the model also adjusts the winds here, leading to directional biases in the output. This problem is not a serious one because the model run usually ends before the bias begins to appear in the windfield (Lanicci and Weber[24]). Lanicci[23] showed that the model produces different windfields for vegetated and nonvegetated areas under light wind conditions. If no vegetation data are available for a location, the model wind output can be suspect for light wind cases.

4.3.2 INTERPRETATION OF VERTICAL WINDSPEED PROFILES

The vertical windspeed profile produced by the model was briefly discussed in Section 3.2.3. Recall the surface-layer wind profiles shown in Figure 9. The model profiles are produced over the surface layer, which is assumed to be 100 m deep during the daytime (on the average). During the day, the windspeed increases

rapidly with height over the lowest 30 to 40 m, then begins to level off from 40 to 100 m. Since the computation height is equal to 10 m, the model-derived profile reflects this rapid increase with height, and maintains it through the entire 100-m layer (see example from model output, shown in Figure 13). This model-generated profile has a tendency to overestimate the winds at levels above 10 m, as will be documented in Section 5. An alternate method of generating these profiles based on a computation height of 31.6 m (the geometric mean of 10 and 100 m, recommended by Panofsky and Dutton[12]), will be discussed in Section 5. Those users who have a need for vertical windspeed profiles should read the next section.

At night, it is not a straightforward task to produce representative wind profiles. Recalling Figure 9 again, the vertical windspeed profile is very sharp, and depends upon the level of the nocturnal jet (for which the model cannot account). Therefore, except for neutral conditions (for which the winds are fairly uniform with height even at night), the model wind profiles are very suspect at night. An example of such a nighttime profile generated by the model is shown in Figure 14. Notice that even for light surface winds of 2-3 ms^{-1}, the model profile produces windspeeds in excess of 20 ms^{-1} only 100 m above the surface. We present the following guidelines for use of the model profiles under nighttime (stable) conditions:

(1) Check the winds and temperatures on the latest available sounding to get estimates of low-level winds and location of the temperature inversion. Also check other data sources such as pilot balloons, pilot reports, numerical model products, and so on, for low-level winds.

(2) In your local area, watch for signs of the presence of a temperature inversion (light surface winds, clear skies, and so on). During the colder months, a snow cover will help the inversion formation through strong radiational cooling after sunset. Watch for other signs such as smoke from fireplaces and woodstoves beginning to reduce visibility. Also, smoke from tall stacks will show a pattern where it rises and fans out when inversions are present. In the early morning, the presence of a shallow haze/smoke layer is another good visual indicator of the inversion layer.

(3) After performing steps 1 and 2, run the model and plot the profile. If the inversion height is near 100 m, the trend of the model wind profile may be reliable, and perhaps just the speed at the top of the profile needs to be reduced. If the top of the inversion layer is more like 200 m or greater, the profile is probably inaccurate, especially if the windspeed at the top of the profile exceeds the windspeeds obtained in step 1.

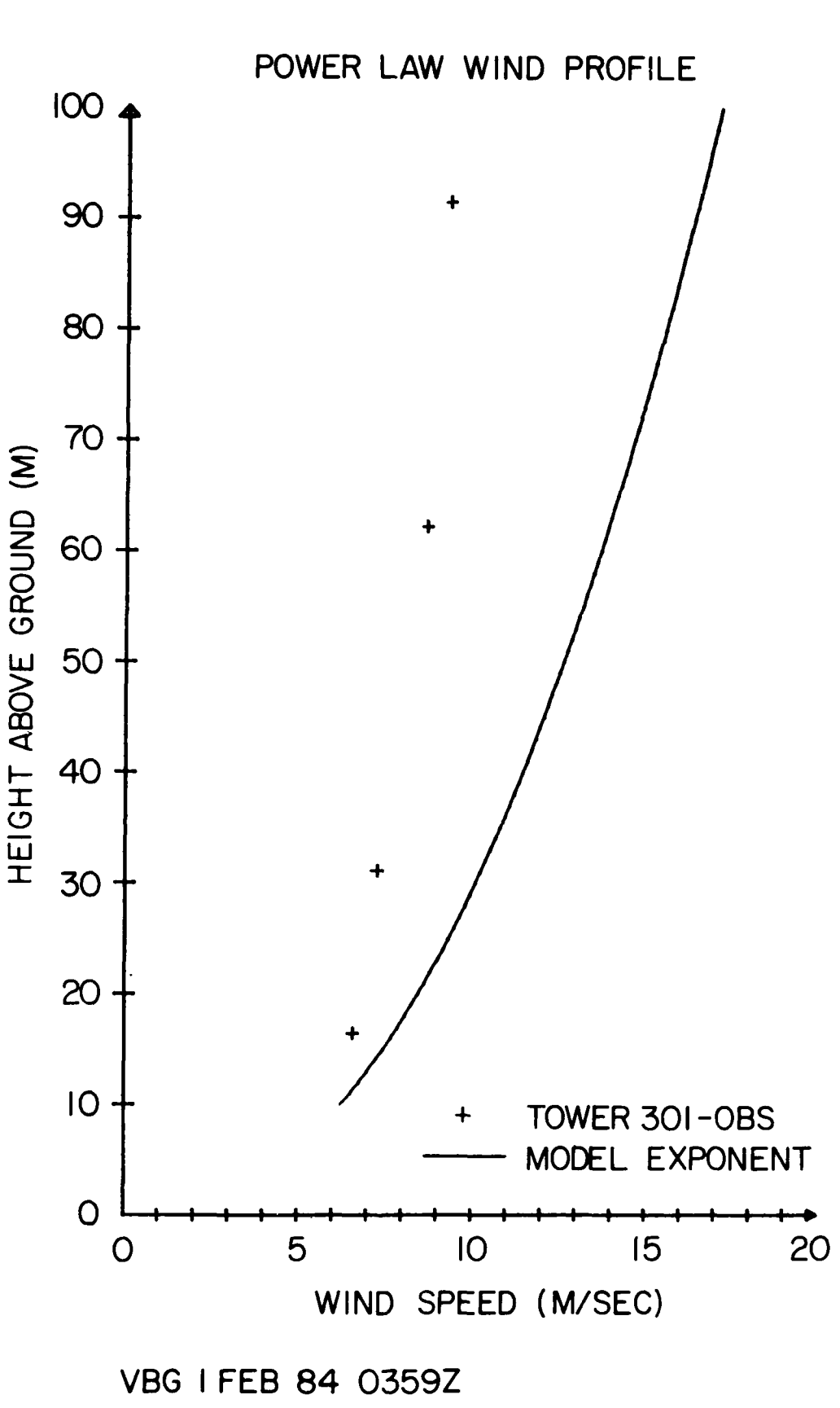

Figure 13. Windspeed Profile Through Lowest 100 m From Vandenberg AFB for 1 February 1984 at 0395Z. Curve is shown for model-generated wind profile. Symbol (+) is observed windspeeds at Vandenberg Tower 301 (along the coast of South Vandenberg

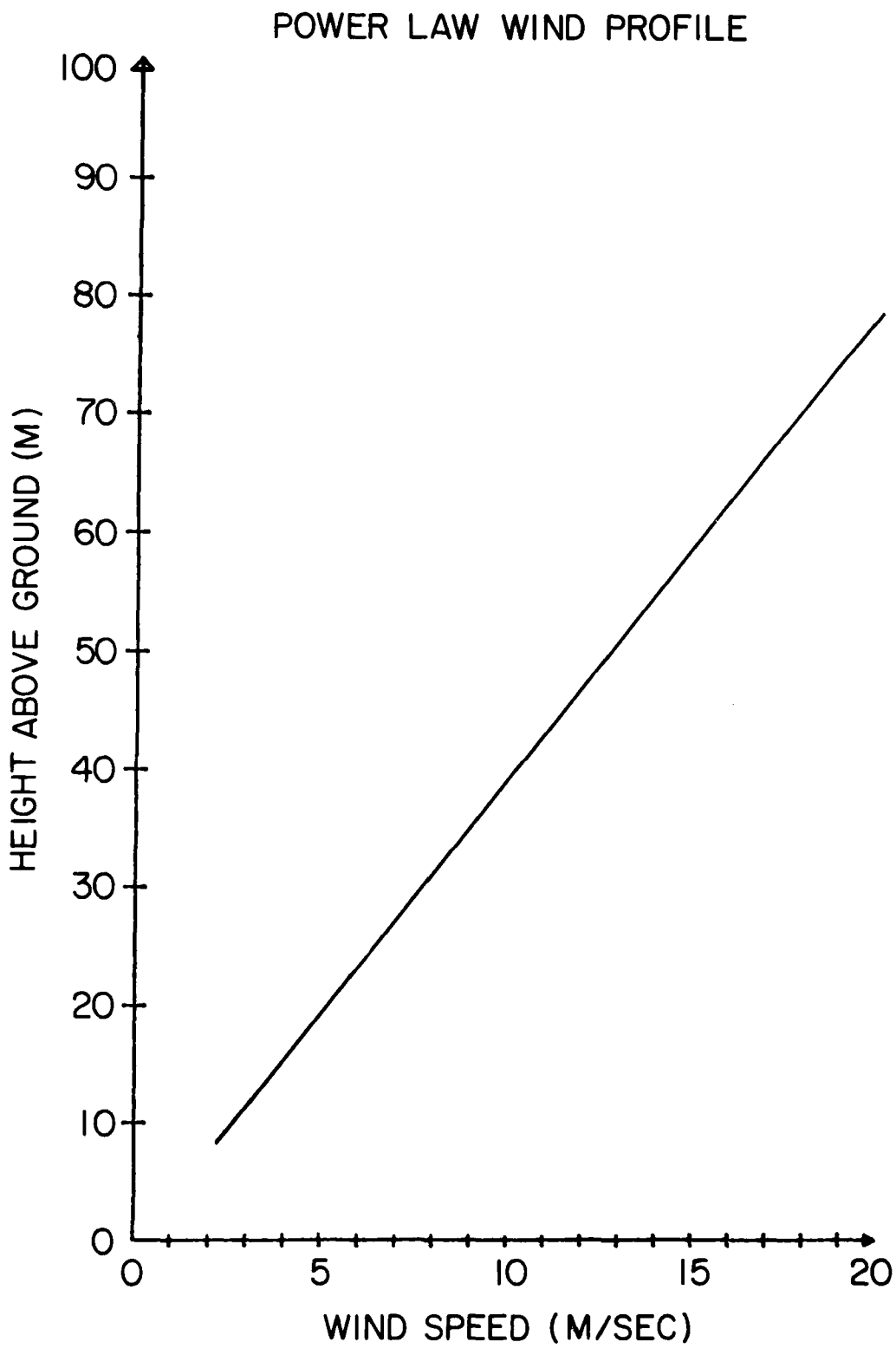

Figure 14. Model Windspeed Profile Generated for Stable Conditions at Ft. Devens, Massachusetts

5. APPLICATION OF THE MODELING SYSTEM TO WEATHER SUPPORT OPERATIONS AT FT. DEVENS, MASSACHUSETTS

This section documents the field test we conducted at the Air Weather Service (AWS) Detachment at Ft. Devens, Massachusetts from mid-September to early November 1986. We first discuss the organization and operational mission of Detachment 12 (Det 12), then the forecaster training that was conducted. We next describe the model windflow climatology generated over Ft. Devens for the month of August. We conclude the section with an outline of the operational tests conducted with the model at the Turner Drop Zone Tactical Training Area (Turner DZ). A summary of each individual case for the Turner DZ tests is presented in Appendix A. We recommend that operational forecasters read Appendix A to get acquainted with the methods we used to determine appropriate input conditions for running the model in real time on a day-to-day basis.

5.1 Detachment 12 Mission and Forecaster Training

Detachment 12 is essentially a two-faceted operation. The base weather station, located at Moore Army Airfield (Moore AAF), is primarily responsible for preparing the TAF and briefing aircrews who transit the area. The Special Operations Weather Team (SOWT) supports Det 12's primary customer, the Army 10th Special Forces Group (10 Group). The SOWT deploys with the 10th Group on exercises and missions, and supports paradrop training that takes place at Turner DZ, located 11 km southwest of Moore AAF. The SOWT consists of four jump-qualified AWS personnel; three forecasters and one observer/forecaster apprentice.

As one might expect, the winds measured at the base weather station (Moore AAF) do not always agree with the winds measured at Turner DZ, because of the 11-km separation. Another problem with the wind measurements at Moore AAF is that, due to terrain effects, windspeeds for directions of west-northwest through north-northeast are consistently underestimated by the equipment by 2 to 4 kt. Forecasters typically add 5 kt to the TAF wind forecast to account for this problem. In Section 5.2, we describe our efforts to simulate this windflow using the model and three-dimensional depictions of the terrain surrounding Moore AAF and Turner DZ.

The weather support given by the SOWT to the 10th Group consists mainly of weather forecasts and observations for Turner DZ, and climatologies for deployment locations as well as potential "hot spot" areas around the world. The 10th Group's paradrop mission is perhaps the most weather sensitive of all the missions they have. They are particularly vulnerable to winds; surface windspeeds (including

gusts) ≧ 13 kt or drop altitude [(900 to 1250 ft AGL for personnel; 1700 ft AGL for cargo)] windspeeds ≧ 30 kt essentially curtail operations for as long as these conditions persist. Wind chill effects are another consideration (chill factors ≦ -25°F are the criteria here). Thus, wind forecasts have an important impact on 10th Group's ability to accomplish its mission. In particular, the windspeed criteria presented are sensitive values that are not easy to predict. It appears that the SOWT's missions are well-suited for application of our windflow modeling system.

The paradrop operation's sensitivity to the wind needs to be further discussed. Nearly every aspect of the operation, from the placement of marker panels over the DZ, to the well-being of the troops once they have landed, is sensitive to the wind direction and speed. The DZ is usually set up over an open field area approximately 1/2 km^2 or greater. Marker panels are placed over the DZ area to give the aircraft commander a landmark he can use to guide the aircraft into the DZ. The markers also give the jumpmaster (the individual responsible for releasing the troops from the aircraft) an idea when he can release his troops to begin their jumps. The timing of the jumpmaster's release of his troops is affected by headwinds or tailwinds over the DZ. It is during the latter part of the jump that the winds are perhaps most crucial when, about 300-ft AGL, the jumper begins to turn his body into the wind. Even a light wind can mean the difference between a safe, soft landing, and an injury resulting from a hard landing or a drift into the treetops.

Currently, the SOWT has several means for estimating winds relative to advising go or no-go decisions for a jump. The first way is through the TAF wind forecast that provides surface wind forecasts up to 24 h before a jump. Another way is through use of a forecast study prepared for Ft. Devens that uses a nomogram giving the surface wind speed at the drop zone as a function of the pressure gradient and the wind direction derived from the latest surface analysis (this nomogram is shown in Figure 15). The third way, most commonly used, is the computation of a layer-mean wind (surface to 1250-ft AGL, usually) by tracking a 10-g balloon launched about 1-1.5 h prior to time-on-target (TOT), and supplemented by surface wind observations taken at the DZ by the DZ Safety Officer using handheld equipment. The layer-mean wind is computed through knowledge of the balloon's ascent rate, and azimuth and elevation angle above the surface as measured with a scope. None of these methods provide wind profile data at different levels. Although the model wind profiles described in Section 4.3 only extend to 300 ft AGL, there are three points we believe should be made about the usefulness of the model wind profiles. First, recall that the lowest 300 ft are the most important in a jump (as previously explained). Second, the drop altitudes in wartime deployment would be closer to 500 ft AGL. Third, future parachute equipment

is being designed for safe operational drops at heights as low as 300 ft AGL (Harclerode[57]). The use of this future equipment could be adequately supported by the surface-layer wind profiles produced by our model.

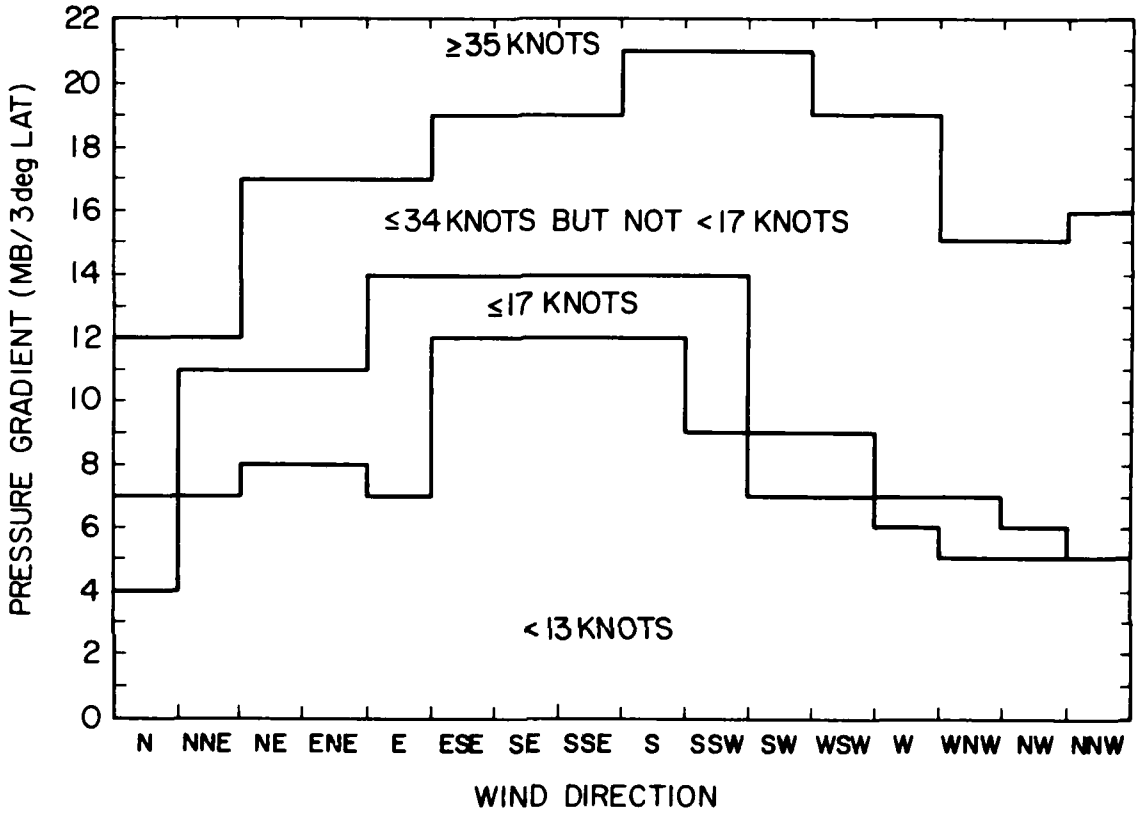

Figure 15. Nomogram Describing Wind Forecast Technique for Turner DZ Operations. A three-degree latitude interval is oriented over surface analysis until strongest pressure gradient over the station is identified. Windspeed is obtained by reading corresponding pressure gradient value and wind direction from surface analysis. This method yields the interval for maximum surface wind gust for a 3 h period following the analysis time

Forecaster training on the windflow modeling system consisted of six sessions using Det 12's Z-100 computer. There were three different programs on which forecasters were trained (see also Section 3). The first one was the windflow model itself, configured to run interactively with the user (see Figure 11 and Section 4.2).

57. Harclerode, P. (1986) GQ's 8 metre low-level parachute, Special Force Journal 1:833-850.

Forecasters provided input data either from current observations, the TAF, or most frequently the TAF updated with current observations. The next program was a horizontal wind plot, that automatically read in the output files from the model. The plot program has two display options: winds depicted by arrows whose length is proportional to speed, or the standard wind plot with barbs. An example of the screen display for the first DZ case (17 September 1986) is shown in Figure 16. A terrain contour display, also shown, was provided so the user could identify

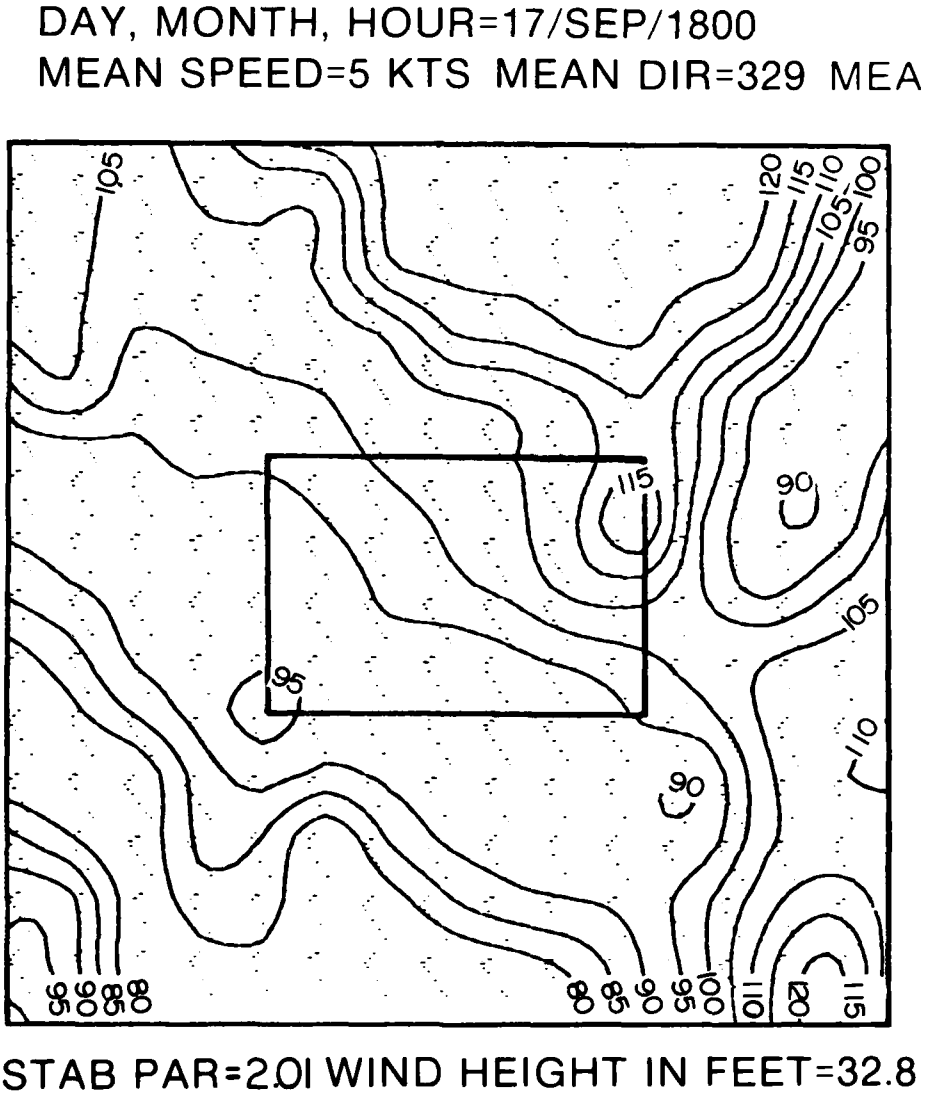

Figure 16. Model Horizontal Wind Plot From Z-100 Screen for 17 September 1986 at 1800Z. Mean wind direction and speed are displayed at top, as is mean value of model-generated profile exponent. Stability parameter is shown at bottom. Terrain overlay is from 3 × 3 km window surrounding Turner DZ

geographic reference points over the model display window. The third program was a vertical windspeed profile display over the lowest 300-ft AGL. In Section 4.3.2 we mentioned that the model-generated wind profiles tended to overestimate the winds at levels above the 10-m computation height (recall Figure 13). To use the profiles for real-time support of Turner DZ operations, we developed a scheme based on calculating the wind profiles using a representative height of 31.6 m (the geometric mean of 10 m and 100 m). This method, shown in Figure 17, yields more reasonable values of the wind profile exponent than those based on the model run. To illustrate this, let us take the 17 September case whose wind plot is shown in Figure 16 and derive the wind exponent for use in the profile program. The stability class from Figure 16 is about 2.01, which is below 3.3; therefore, conditions are unstable, and from Figure 17, the exponent is 0.16. The model-generated exponent, also shown in Figure 16, is 0.31, which is almost twice the derived value. Plots of the wind profile using the model-generated exponent and the derived exponent are shown in Figures 18a and 18b, respectively. A comparison of the two profiles shows that the modified profile is flatter than that generated by the model, with a 300-ft windspeed of 7 kt, as opposed to 10 kt from the model. The Mean Effective Wind (MEW) as measured for this case was 310°/10 kt, so that the modified profile is slightly more consistent with the Mean Effective Wind than is the model-generated profile. For all of the 13 jump operations for which we provided model support, the windspeed profiles based on Figure 19 were more consistent with ground- and balloon-based measurements than those derived from the model exponent. We should note here that none of our 13 cases had stable conditions, and the profile's reliability is still suspect under these conditions (recall Section 4.3.2).

All of the personnel whom we trained agreed that the windflow modeling system was easy to learn and use, and that the system was a valuable addition to SOWT support at Turner DZ.

5.2 Model Windflow Climatology Simulations for August

In order to demonstrate the uses for the windflow model in a deployment scenario, we generated windflow climatology over the Ft. Devens reservation, using August climate data from the Terminal Forecast Reference Notebook (TFRN). The TFRN is a standard AWS publication containing station climatology and local forecast studies. The model was run for the predominant wind directions of southwest and west using various windspeeds for both daytime and nighttime conditions. These wind simulations were run to determine the presence of local terrain effects on the windflow, particularly over Turner DZ and Moore AAF.

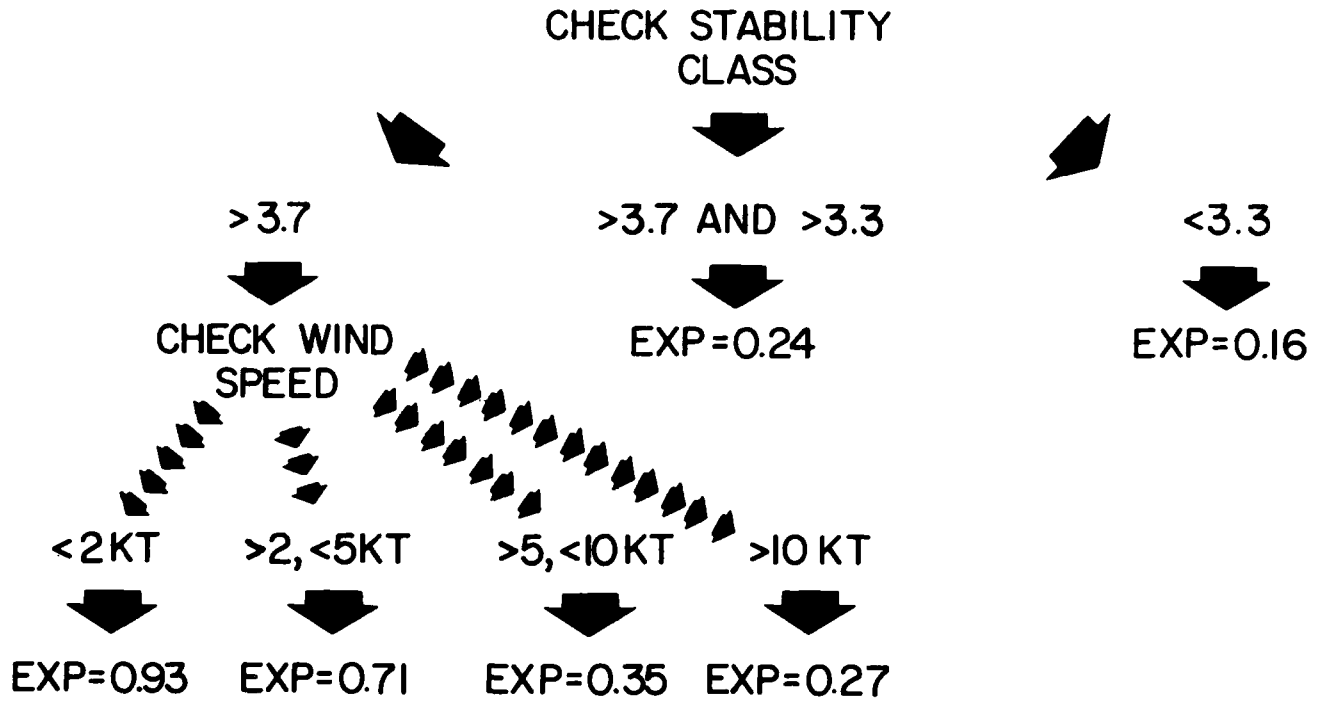

Figure 17. Method for Determining Values of Wind Profile Exponent as a Function of Diagnosed Stability Parameter. Notice that for stable conditions (SP > 3.7), the exponent tends toward the neutral value (0.24) as windspeeds increase

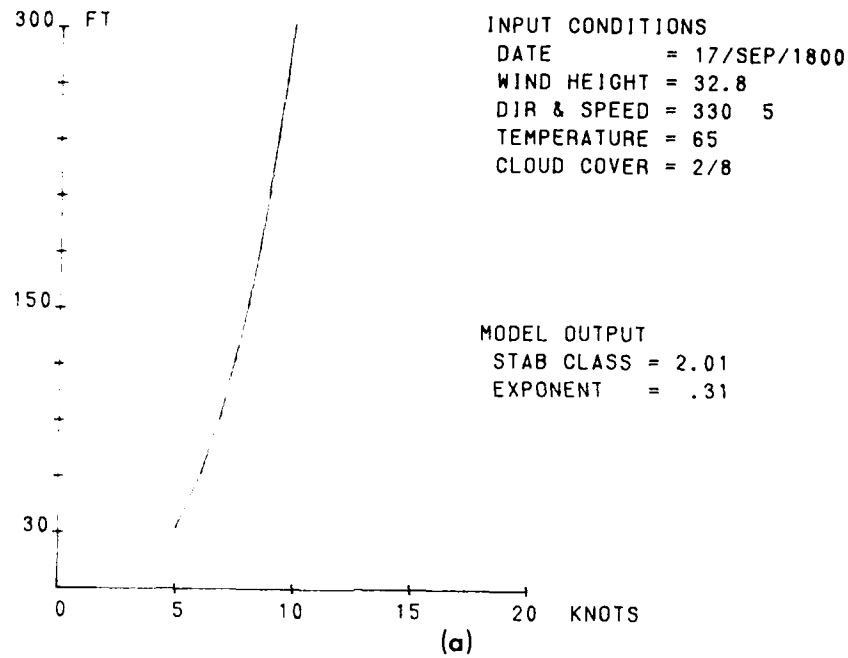

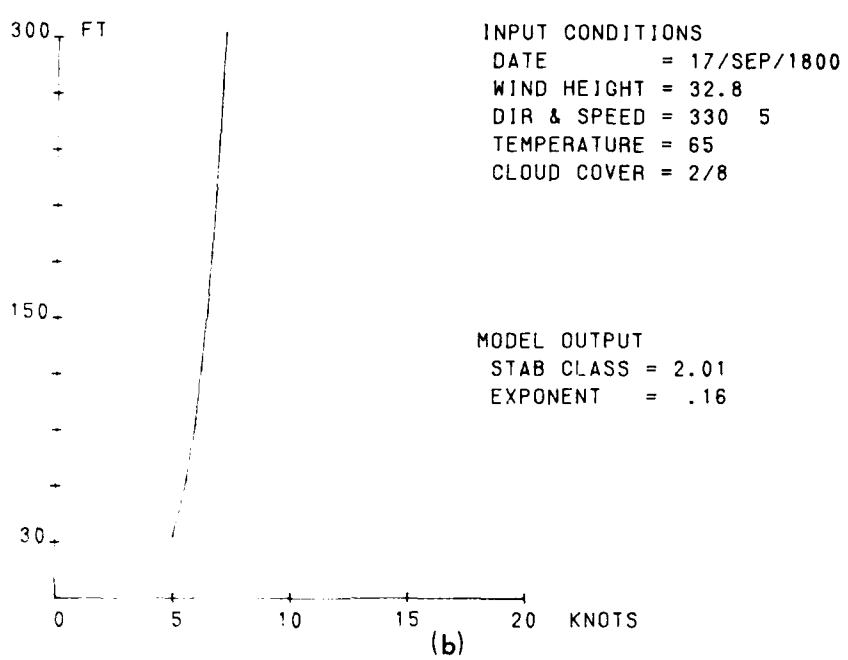

Figure 18. Model Windspeed Profiles for 17 September 1800Z Case. Profiles are shown for: (a) model-generated exponent; and (b) derived exponent

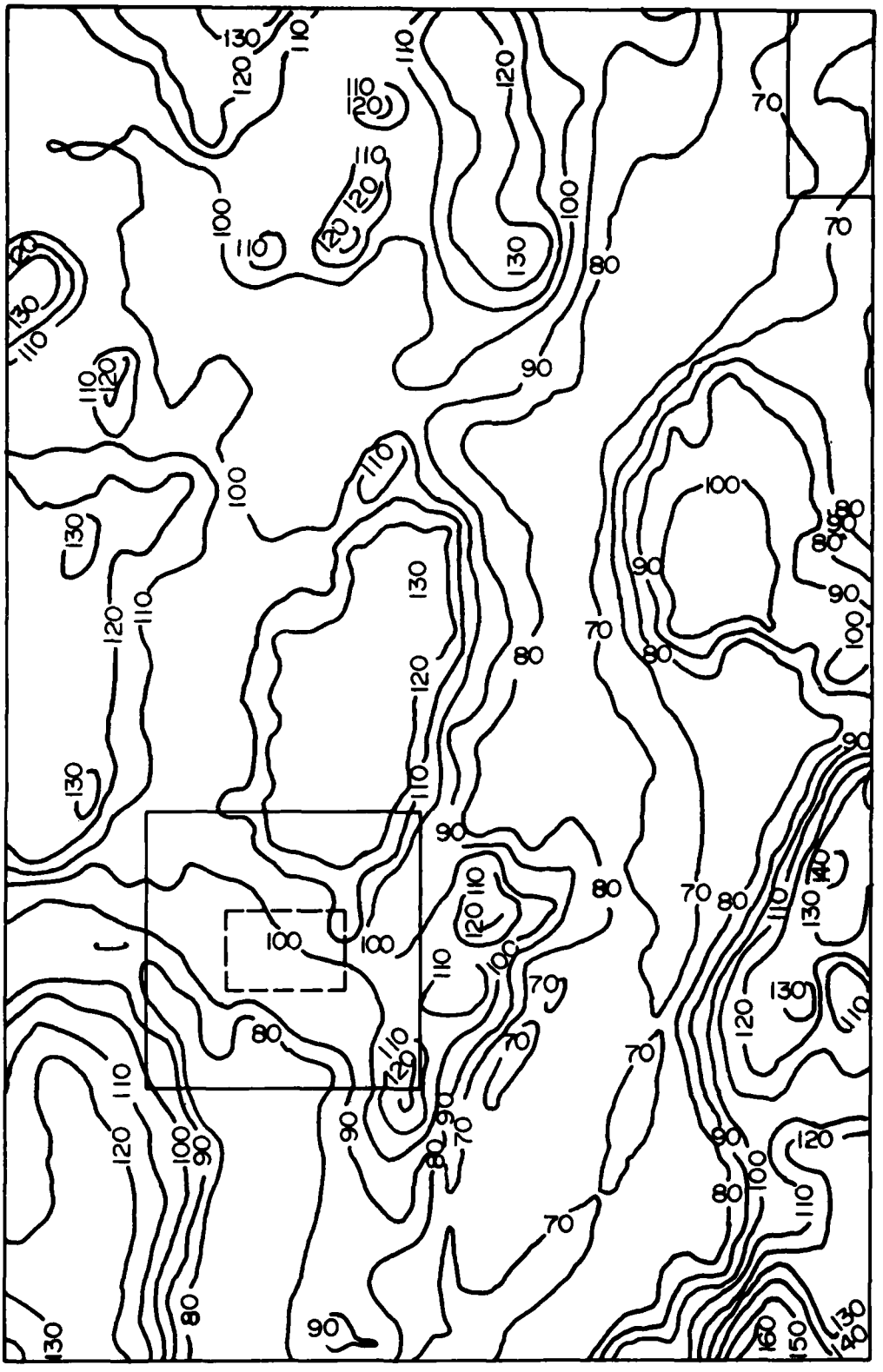

Figure 19. Ft. Devens Model Terrain Elevations in m MSL. The 3 × 3 km window used for the operational model test is in the west-central portion of the model domain. Turner DZ is highlighted by the dashed border within the window. The area surrounding Moore AAF is shown by solid outline of northeast corner of domain

The model domain for the simulations is shown in Figure 19. The domain size was 8.8 km west to east by 13.8 km south to north. With a 200-m horizontal spacing between grid points, this translates into an array 44 × 69 (3036 grid points). Since we had no vegetation height data for this area, we assumed a constant surface roughness of 50 cm, corresponding to gentle topography with some forest cover. Turner DZ (shown by the box in Figure 20) is located in a large open area (900 × 600 m) of sloping terrain. The area is well-exposed to winds with directions from southerly to northwesterly. A small hill (about 115 m above mean sea level MSL) appears in the northeast corner. The terrain slopes to the southwest, from about 115 to 120 m MSL to around 90 m MSL in the southwest corner. The average terrain grade is about 1.7 percent. Vegetation over the DZ consists of tall grasses in a sandy soil. The DZ is surrounded on all sides by mixed coniferous and deciduous trees about 10 to 15 m high. Moore AAF (shown in Figure 21) sits on a small plateau oriented northwest to southeast, about 1.7 km long and 0.8 km wide. The plateau is about 15 to 20 m above the surrounding terrain that consists mainly of forest, several marshes, and the nearby Nashua River.

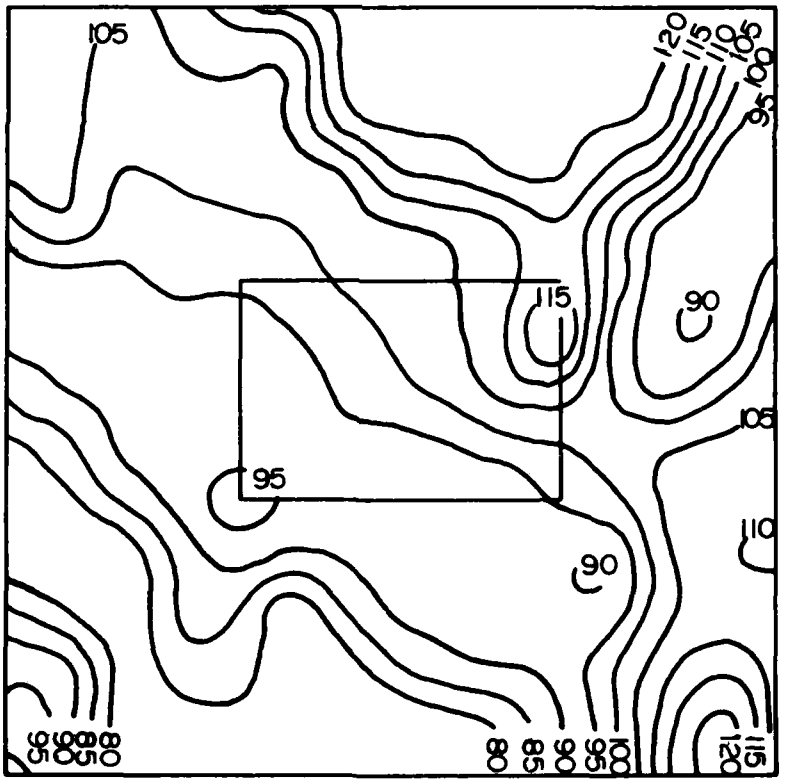

Figure 20. Enlargement of 3 × 3 km Window Used for Model Tests at Turner DZ. The DZ is highlighted by the solid border in the center

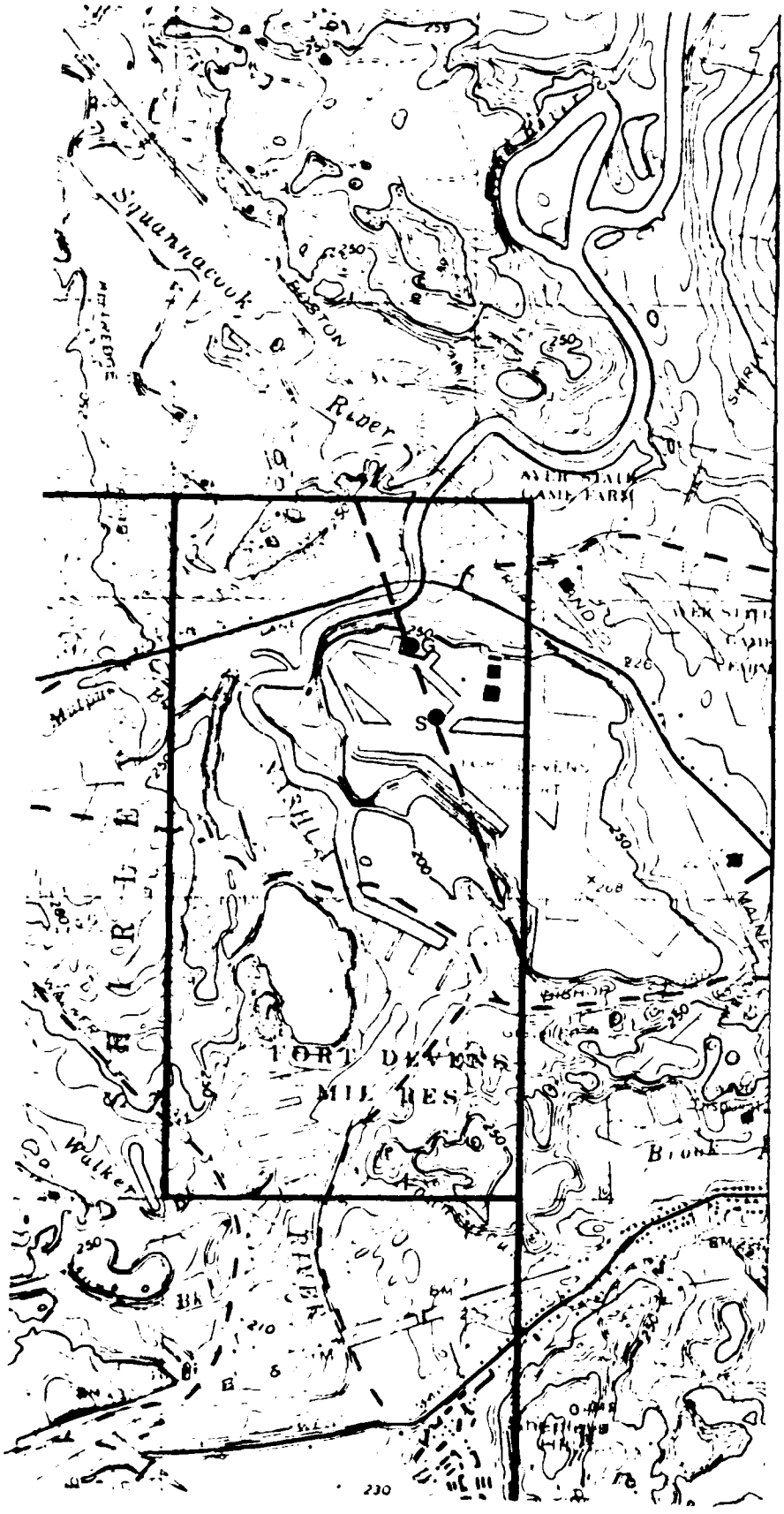

Figure 21. U.S. Geological Survey Map at 1:25,000 Scale Showing Terrain Elevations (in ft MSL) Over Area Surrounding Moore AAF. The "G" denotes the location of GMQ-20 wind-measuring equipment at the north end of the runway. The "S" denotes the location of a windsock some 300 m south-southeast of "G". The dashed line shows the location over which a cross section (Figure 22) was taken to illustrate the flow separation/eddy effect

Recall from Section 5.1 that Moore AAF has a wind equipment problem because of the terrain. We examined the terrain around Moore AAF using horizontal maps and three-dimensional terrain diagrams generated from our terrain elevation data for Ft. Devens. From forecaster interviews and the TFRN, we determined that the wind-measurement problem was being caused by flow separation taking place as the wind encounters the sudden terrain slope at the north end of the airfield. This flow separation was producing small turbulent eddies over the area where the wind equipment was located (see terrain cross section and flow diagram in Figure 22). However, after the flow rides up the plateau's side, it descends about 150 to 200 m downwind of the airfield edge. This descent has been confirmed by hand-held equipment and a wind sock that is located about 300 m downwind of the wind equipment. Flow separation along the edges of escarpments and cliffs has been studied by several researchers, such as Scorer[58,59] and Jones.[60] A concise summary of flow separation and wake effects appears in Orgill.[61] Observations of flow separation show that the zones of turbulent eddies at the edge of a cliff can be 2 to 10-m deep (well above the level of a standard wind measurement system), and can extend about 50 to 200-m downwind. Thus, the observations at Moore AAF are confirmed by other observational studies. The horizontal scale of these eddies is too small to be accounted for by the windflow model. Numerical models can only "recognize" features having a wavelength equal to or greater than four grid spaces. Our model, with a 200-m spacing, can only resolve features with wavelengths 800 m or greater. Another way of phrasing this would be to say that if we wanted to attempt to model this flow separation, we would need a grid spacing of about 50 m (this, of course, does not guarantee that we could simulate this feature simply by reducing the grid spacing).

---

58. Scorer, R.S. (1955) Theory of airflow over mountains: IV-Separation of flow from the surface, Quart. J. Roy. Meteorol. Soc. 81:340-350.

59. Scorer, R.S. (1972) Clouds of the World, Stackpole Books, Harrisburg, PA.

60. Jones, O.K. (1970) The flow of a stratified fluid over a vertical step, Tellus 22(No. 5):481-492.

61. Orgill, M.M. (1981) Atmospheric Studies in Complex Terrain: A Planning Guide for Future Studies, PNL-3656, ASCOT/80/4, Pacific Northwest Laboratory, Richland, Wash., 99352.

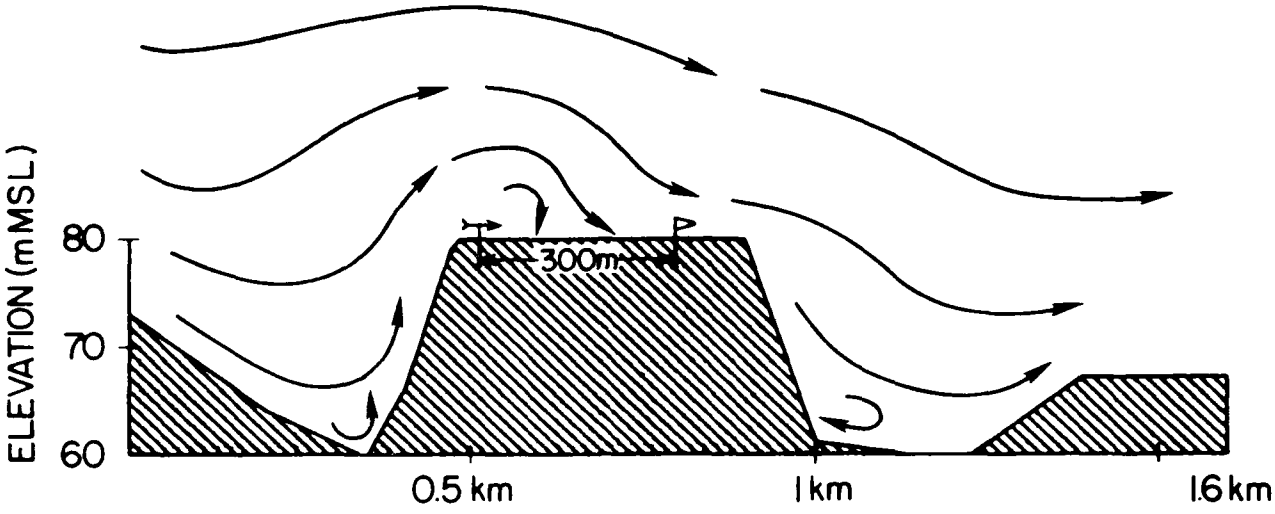

Figure 22. Illustration of Flow Separation/Eddy Effect Occurring With a Wind Direction of 340 . The cross section shows the terrain elevations in m with the streamlines and arrows describing the flow up to about 30 m AGL. The GMQ-20 equipment is depicted by the windvane; the windsock is shown about 300 m downwind

Although the model cannot account for differences in the wind measurements along the runway of Moore AAF, it can give us information about slope wind effects on the flow. We accomplished this by comparing the mean wind directions and speeds for Moore AAF and Turner DZ for each set of climatological simulations. As these mean winds get closer together, the terrain effects can be said to have decreased over the Ft. Devens region. We compared Moore AAF to Turner DZ to see if any systematic wind differences between the two locations could be found. This information would be useful in that a relocation of the wind equipment at Moore AAF would not necessarily eliminate discrepancies in wind measurements between the airfield and the DZ. The results of our wind microclimate simulations appear in Table 6. We are not surprised to see that slope wind effects are only important for windspeeds below 6 kt, and are essentially negligible above 6 kt. Below 6 kt, the winds at Turner DZ are about 1-2 kt stronger than at Moore AAF during the day, but at night the speeds are virtually the same. Wind directions at Turner DZ also tended to be about 10 to 35° more southerly than at Moore AAF during the day. At night, winds at Turner were 5 to 30° more northwesterly than at the airfield. Keep in mind that these simulation results are only applicable for southwesterly and westerly winds at Moore AAF and for essentially clear to scattered conditions. For cloudy, neutral stability conditions, we would expect the differences between the two locations to be smaller. From Table 6 we can conclude

Table 6. Summary of August Wind Climatology Simulations for Ft. Devens (August 15)

Input Wind Dir/Speed	No. Step to Solution	Model Mean Dir/Speed (Max Speed) Moore AAF	Turner DZ
Daytime (1400 LST)			
Input Conditions: Temperature = 80° F, Cloud Cover = 1/8			
270°/1 kt	26	279°/1 kt (2.4)	245°/2 kt (2.7)
270°/4 kt	23	273°/3 kt (4.0)	265°/5 kt (5.0)
270°/6 kt	5	272°/6 kt (6.1)	269°/6 kt (6.3)
270°/8 kt	2	271°/8 kt (8.1)	272°/8 kt (8.1)
270°/16 kt	2	271°/16 kt (16.1)	271°/16 kt (16.3)
225°/4 kt	34	229°/3 kt (3.4)	216°/4 kt (4.2)
225°/6 kt	15	228°/5 kt (5.4)	226°/5 kt (5.6)
225°/8 kt	2	226°/8 kt (8.0)	226°/8 kt (8.1)
225°/16 kt	2	226°/16 kt (16.2)	226°/16 kt (16.2)
Nighttime (2100 LST)			
Input Conditions: Temperature = 70° F, Cloud Cover = 1/8			
270°/1 kt	18	263°/1 kt (2.2)	295°/1 kt (2.2)
270°/4 kt	19	268°/4 kt (5.2)	279°/4 kt (5.2)
270°/6 kt	2	271°/6 kt (6.1)	272°/6 kt (6.1)
270°/8 kt	2	271°/8 kt (8.2)	270°/8 kt (8.2)
270°/16 kt	2	271°/16 kt (16.1)	271°/16 kt (16.3)
225°/4 kt	20	220°/4 kt (5.2)	227°/3 kt (5.2)
225°/6 kt	7	228°/6 kt (6.0)	229°/6 kt (6.0)
225°/8 kt	2	226°/8 kt (8.0)	226°/8 kt (8.0)
225°/16 kt	2	226°/16 kt (16.2)	226°/16 kt (16.2)

that, according to the model, terrain slope effects on the winds can add 1-2 kt to the wind speed differences between Turner DZ and Moore AAF. Adding the differences from wind sensor placement on the runway to this, we find that a reported light wind at Moore AAF may cause problems for jumpers at the DZ as illustrated in the following example.

Daytime (Unstable) Conditions with Scattered Clouds

Moore AAF observation: 270°/5 kt

Turner DZ winds:

(1) Add slope wind effect (-10 to -35°/+1 to 2 kt): 235 to 260°/6-7 kt
(2) Add wind instrument error (+2 to 4 kt) : 235 to 260°/8-11 kt
(3) Compute wind profile exponent (Figure 17) : Exponent = 0.16
(4) Profile winds at 300 ft: 11 to 16 ft (critical windspeeds could be encountered).

The preceding example, though hypothetical, illustrates the usefulness of the model windflow climatology together with other known information to make a determination of safety conditions at the DZ. Situations similar to the above example have actually been observed by SOWT members at the DZ on several occasions. A few of our cases in the next section also illustrate these effects, using both the windflow model output and vertical wind profiles in support of jump operations at Turner DZ.

5.3 Operational Testing for Paradrop Operations at Turner Drop Zone

This section summarizes the operational tests over Turner DZ using the model and its peripheral programs. We followed the guidelines for model input that were outlined in Sections 4.2 and 4.3. The model domain used for this real-time test was a 3 × 3 km window (highlighted by solid lines in Figure 19; window itself shown in Figure 20) surrounding Turner DZ. The window was a 15 × 15 array (225 grid points), and was constrained by the limitations of Det 12's Z-100 computer without the "math chip." As a rule, the model took 12 to 20 min to produce a simulation. Use of TAF information for input enabled the model to be run as a forecast model, giving SOWT forecasters as much as 24 h lead time in examining horizontal winds and vertical profiles for a jump operation.

Operational testing was usually conducted in the following manner. A preliminary ("first look") model run was made as much as 24 h prior to a jump using input from the TAF. On the morning before the scheduled jump (most jumps were in the afternoon, but we had two night jumps), we reran the model using the latest TAF updated with current observations. We sometimes ran the model more than once using the most current observations. Approximately 3 to 6 h prior to TOT we chose the model run we believed was most accurate and used it for supporting that day's operation. This method allowed us to begin looking at forecast conditions over the DZ the day before a jump, and enabled us to "metwatch" DZ conditions right up until the time of balloon launch 1-1.5 h before TOT.

The summary of our operational testing is shown in Table 7. There are several interesting results from the evaluation. First, notice that the model wind profile indicated 300 ft winds in excess of the critical surface value on five occasions. On four of these occasions wind gusts greater than 13 kt were reported at the DZ and on a fifth occasion (28 October 1500Z), gusts in excess of critical speed appeared about 1.5 h after verification. The model wind profiles showed these strong winds aloft despite the fact that neither the input TAF nor the model surface wind plot indicated windspeeds $\geq$ 13 kt. We believe that the model wind profiles can be used to predict gusty surface winds over the DZ because the winds from aloft can be mixed down to the surface through turbulent eddy processes (recall Section 4.1). Another interesting result of our evaluation is that the model correctly diagnosed the stability as neutral instead of stable, for the two nighttime cases (2 and 3) that had stratocumulus cloud decks. This correct stability diagnosis led to model wind profiles that agreed well with the measured mean effective winds. Notice from Table 7 that there were also several occasions (cases 4, 7, 9) that behaved similarly to our example presented at the end of the last section. The most dramatic case was No. 4, where a 10 kt difference was observed between Moore AAF and Turner DZ. The wind direction at the DZ was 50° less than at the airfield, and surface gusts in excess of the critical value were observed at the DZ. In all three cases, the wind trajectories were from the west to northwest and were consistent with the flow separation theory discussed in the previous section and described in the schematic diagram of Figure 22. This last result illustrates the benefits from producing model wind climatologies and combining the results with other known information about the station.

Although the results documented in Table 7 look impressive, we should make several cautionary points about our study. First, this is a small sample size (13 cases) that consisted mainly of neutral cases. For stable cases, we advise caution in the interpretation of the model profiles. We would expect some model "false alarms" to appear in a larger data sample. We must also remember that the model output is only as good as the TAF or updated information that is put into the model. Notice from Table 7 that the greatest error between input and observed DZ windspeeds was only about 5 kt (cases 2 and 12). This was due to the quality TAFs we received and the diligent updates that were made before running the model.

Table 7. Summary of Turner Drop Zone Operational Tests

Case No.	Date/Time	Initial Conditions				Output			Verification			
		Source	Winds	Cloud Cover (Type)	Temp	Stability	Winds	Calculated 300 ft Windspeed	DZ Winds	AAF Winds	MEW	Critical Winds Observed?
1	17 Sep/1800Z	11Z TAF	330°/5 kt	2/8	65°F	Unstable	329°/5 kt	7 kt	310°/5 kt	010°/2 kt	310°/10 kt	No
2	17 Oct/0100Z	16 Oct 17Z TAF	290°/5 kt	7/8 (Sc)	46°F	Neutral	294°/5 kt	9 kt	Calm	23Z: Calm	350°/12 kt	No
3	18 Oct/0630Z	17 Oct 17Z TAF	010°/5 kt	7/8 (Sc)	38°F	Neutral	009°/5 kt	9 kt	025°/2-3 kt	Closed	015 /6 kt	No
4	24 Oct/1800Z	11Z TAF	350°/10 kt	3/8	57°F	Unstable	350°/11 kt	16 kt*	300°/10-11 kt w/gusts	350°/1 kt	320°/11-12 kt	Yes
5	26 Oct/1500Z	15Z Area Obs	350°/1 kt	8/8 (As)	46°F	Unstable	306°/1 kt	1 kt	Calm	Calm	Lgt/Var	No
6	28 Oct/1300Z	27 Oct 18Z TAF	300°/5 kt	8/8 (Fog)	51°F	Neutral	304°/5 kt	9 kt	270°/6 kt	Calm	290°/12 kt	No
7	/1550Z	27 Oct 18Z TAF	330°/8 kt	7/8 (Fog)	51°F	Neutral	332°/9 kt	15 kt*	300°/5 kt	270°/3 kt	295°/2 kt	No[2]
8	29 Oct/1900Z	28 Oct 18Z TAF	240°/10 kt	4/8	68°F	Neutral	243°/10 kt	17 kt*	210°/10-12 kt w/gusts	240°/9 kt gusts to 19 kt	250°/14-15 kt	Yes
9	30 Oct/1430Z	12Z TAF Post-Frontal Conditions for 17Z)	290°/12 kt	3/8	60°F	Neutral	293°/12 kt	20 kt*	14Z: 300°/11 kt w/gusts	14Z: 290°/6 kt	295°/14 kt	Yes
10	/1630Z	Same as 9	290°/12 kt	3/8	60°F	Neutral	293°/12 kt	20 kt*	16Z: 320°/10 kt gusts to 15	16Z: 330° 7 kt gusts to 12 kt	320°/12 kt[2]	Yes
11	03 Nov/1800Z	12Z TAF	180°/7 kt	1/8	51°F	Unstable	180°/7 kt	10 kt	180°/5 kt	190°/3 kt	175 /8 kt	No
12	05 Nov/1800Z	12Z TAF	040°/7 kt	7/8 (Ac)	39°F	Neutral	037°/7 kt	12 kt	045°/1-3 kt	060°/2 kt	085 /5 kt	No
13	07 Nov/1900Z	12Z TAF	220°/5 kt	7/8 (St)	50°F	Neutral	224°/5 kt	9 kt	220°/6 kt	260°/1 kt	245 /6 kt	No

*300 ft windspeed ≥ 13 kt

1 layer mean of surface to 1100 ft AGL

2 at 1630Z, DZ windspeeds had increased to 12 kt, with higher gusts reported.

References

1. Anthes, R.A., and Warner, T.T. (1978) The development of mesoscale models suitable for air pollution and other mesometeorological studies, Mon. Wea. Rev. 106:1045-1078.
2. Mahrer, Y., and Pielke, R.A. (1977) The effects of topography on sea and land breezes in a two-dimensional numerical model, Mon. Wea. Rev. 105:1151-1162.
3. Tripoli, G.J., and Cotton, W.R. (1982) The Colorado State University three-dimensional cloud/mesoscale 1982. Part I: General theoretical framework and sensitivity experiments, J. Rech. Atmos. 16:185-219.
4. Danard, M. (1977) A simple model for mesoscale effects of topography on surface winds, Mon. Wea. Rev. 105:572-581.
5. Mass, C.F., and Dempsey, D.P. (1985) A one-level, mesoscale model for diagnosing surface winds in mountainous and coastal regions. Mon. Wea. Rev. 113:1211-1227.
6. Alpert, P., Eppel, A., and Getenio, B. (1985) Surface wind prediction over complex terrain - Application of a one-level terrain following model to Israel, Preprints Seventh Conf. Numerical Weather Prediction, Am. Meteorol. Soc., Boston, Mass., pp. 369-373.
7. Pielke, R.A. (1982) The role of mesoscale numerical models in very-short-range forecasting, in Nowcasting, K.A. Browning, Ed., Academic Press Inc., New York.
8. Ball, J.A., and Johnson, S.A. (1978) Physically Based High Resolution Surface Wind and Temperature Analysis for EPAMS, ASL-CR-78-0043-1, U.S. Army Atmospheric Sciences Laboratory, White Sands Missile Range, N. Mex., ADA 055861.
9. Svejkovsky, J. (1985) Santa Ana airflow observed from wildfire smoke patterns in satellite imagery, Mon. Wea. Rev. 113:902-906.
10. Cionco, R.M. (1983) On the coupling of canopy flow to ambient flow for a variety of vegetation types and densities, Boundary - Layer Meteorol. 26:325-335.

References

11. Cionco, R. M. (1985) On modeling canopy flow coupled to the surface boundary layer, Proc. 17th Conf. on Agriculture and Forest Meteorology and 7th Conf. on Biometeorology and Aerobiology, Am. Meteorol. Soc., Boston, Mass., pp. 116-119.

12. Panofsky, H. A., and Dutton, J. A. (1984) Atmospheric Turbulence: Models and Methods for Engineering Applications, Wiley, New York, 297 p.

13. Kirchoff, R. H., and Kaminsky, F. C. (1983) Empirical Modeling of Wind Speed Profiles in Complex Terrain, DOE-ET/10374-82/1 (DE 83011613), Pacific Northwest Laboratory (Contract DE-AC06-76RLO 1830), Richland, Wash., 99352.

14. Barnard, J. C., Weglev, H. L., and Hiester, T. R. (1985) Improving the Performance of Mass-Consistent Numerical Models Using Optimization Techniques, PNL-5566 (Contract DE-AC06-76RLO 1830), Pacific Northwest Laboratory, Richland, Wash., 99352.

15. Tabony, R. C. (1985) Relations between minimum temperature and topography in Great Britain, J. Climatology 5:503-520.

16. Cionco, R. M. (1982) A meteorological approach to chemical defense over complex terrain with vegetation, Workshop on the Parameterization of Mixed-Layer Diffusion, Las Cruces, N. Mex., pp. 323-328.

17. Ohmstede, W. D. (1982) The parameterization of battlefield dispersion-new frontiers, Workshop on the Parameterization of Mixed-Layer Diffusion, Las Cruces, N. Mex., pp. 279-287.

18. Ohmstede, W. D., and Stenmark, E. B. (1982) A model for characterizing transport and diffusion of air pollution in the battlefield environment, Workshop on the Parameterization of Mixed-Layer Diffusion, Las Cruces, N. Mex., pp. 416-423.

19. Amlicke, B. B., and Coleman, I. W. (1984) High Resolution Wind (HRW) Model, MRC/WDR-R-089, Mission Research Corporation, Alexandria, VA.

20. Cionco, R. M. (1985) Modeling airflow over variable terrain, Proc. of the HAZMAT '85 West Conference, Long Beach, Calif.

21. Veazey, D. R., and Tabor, P. A. (1985) Meteorological sensor density on the battlefield, Workshop on Geographic Information Systems in Government, Bruce Opitz (Ed.), Deepak Publishing, Hampton, VA, pp. 195-208.

22. Weber, H. (1986) private communication.

23. Lanicci, J. M. (1985) Sensitivity Tests of a Surface-Layer Windflow Model to Effects of Stability and Vegetation, AFGL-TR-85-0265, ADA 169136.

24. Lanicci, J. M., and Weber, H. (1986) Validation of a Surface-Layer Windflow Model Using Climatology and Meteorological Tower Data from Vandenberg AFB, California, AFGL-TR-86-0210, ADA 178480.

25. Lanczos, C. (1970) The Variational Principles of Mechanics (4th Ed.) U. of Toronto Press, Toronto, pp. 106-110.

26. Sasaki, Y. (1958) An objective analysis based on the variational method, J. Meteorol. Soc. Japan 36:77-88.

27. Sasaki, Y. (1970) Some basic formalisms in numerical variational analysis, Mon. Wea. Rev. 98:875-883.

28. Haltiner, G.J., and Williams, R.T. (1980) Numerical Prediction and Dynamic Meteorology (2nd Ed.), Wiley and Sons, New York, 447 p.

29. Dutton, J.A. (1976) The Ceaseless Wind, McGraw-Hill, New York, pp. 435-439.

30. Atkinson, B.W. (1981) Mesoscale Atmospheric Circulations, Academic Press, London, pp. 252-254.

31. Turner, D.B. (1964) A diffusion model for an urban area, J. Appl. Meteorol. 3:83-91.

32. Kunkel, B.A. (1985) Development of an Atmospheric Diffusion Model for Toxic Chemical Releases, AFGL-TR-85-0338, ADA 169135.

33. List, R.J., Ed. (1958) Smithsonian Meteorological Tables (Vol. 114) Smithsonian Miscellaneous Collections.

34. Smith, F.B. (1972) A scheme for estimating the vertical dispersion of a plume from a source near ground level, Proc. of the Third Meeting of the Expert Panel on Air Pollution Modeling, NATO Committee on the Challenges of Modern Society, Paris, France.

35. Ragland, K.W., and Dennis, B.L. (1975) Point source atmospheric diffusion model with variable wind and diffusivity profiles, Atmos. Environ., 9:175-189.

36. Golder, D. (1972) Relations among stability parameters in the surface layer, Boundary Layer Meteorol. 3:47-58.

37. USNRC (1972) Onsite Meteorological Programs Regulatory Guide 1.23, U.S. Nuclear Regulatory Commission.

38. Sedefian, L., and Bennett, E. (1980) A comparison of turbulence classification Schemes, Atmos. Environ. 14:741-750.

39. Businger, J.A., Wyngaard, J.C., Izumi, Y., and Bradley, E.F. (1971) Flux-profile relationships in the atmospheric boundary layer, J. Atmos. Sci. 28:181-189.

40. Gringorten, I.I., and Grantham, D.D. (1983) Winds as a Function of Height, in Winds: Chapter 6, 1983 Revision, Handbook of Geophysics and Space Environments, AFGL-TR-83-0080, AD A132018.

41. McNider, R.T., and Pielke, R.A. (1984) Numerical Simulation of slope and mountain flows, J. Climate and Appl. Meteorol. 23:1441-1453.

42. McNider, R.T. (1982) A note on velocity fluctuations in drainage flows, J. Atmos Sci. 39:1658-1660.

43. Banta, R.M. (1986) Daytime boundary-layer evolution over mountainous terrain. Part II: Numerical studies of upslope flow duration, Mon. Wea. Rev. 114:1112-1130.

44. Anderson, G.E. (1971) Mesoscale influences on windfields, J. Appl. Meteorol. 10:377-386.

45. Dickerson, M.H. (1978) MASCON - A mass-consistent atmospheric flux model for regions with complex terrain, J. Appl. Meteorol. 17:241-253.

46. Sherman, C.A. (1978) A mass-consistent model for wind fields over complex terrain, J. Appl. Meteorol. 17:312-319.

47. Fox, D.G., Fosberg, M.A., Marlatt, W.E., and Reeser, W. (1976) Analysis of mountain air quality, Proc. of Third Symposium on Atmospheric Turbulence, Diffusion, and Air Quality, Am. Meteorol. Soc., Boston, Mass., pp. 470-475.

48. Goodin, W.R., McRae, G.J., and Seinfeld, J.H. (1980) An objective analysis technique for constructing three-dimensional urban-scale windfields, J. Appl. Meteorol. 19:98-108.

49. Anthes, R.A., Panofsky, H.A., Cahir, J.J., and Rango, A. (1978) The Atmosphere (2nd Ed.), Merrill Publishing Co., Columbus, Ohio, pp. 128-131.

50. Wyngaard, J.C. (1985) Structure of the planetary boundary layer and implications for its modeling, J. Climate and Appl. Meteorol. 24:1131-1142.

51. Uccellini, L.W., and Johnson, D.R. (1979) The coupling of upper and lower tropospheric jet streaks and implications for the development of severe convective storms, Mon. Wea. Rev. 107:682-703.

52. Means, L.L. (1944) The Nocturnal Maximum of Thunderstorms in the Midwestern States, Miscellaneous Report 16, University of Chicago.

53. Lettau, H.H. (1954) Graphs and Illustrations of Diverse Atmospheric States and Processes Observed During the Seventh Test Period of the Great Plains Turbulence Field Program, Occasional Report No. 1, Atmospheric Analysis Laboratory, Air Force Cambridge Research Center.

54. Blackadar, A.K. (1957) Boundary-layer wind maxima and their significance for the growth of nocturnal inversions, Bull. Am. Meteorol. Soc. 38:283-290.

55. Pitchford, K.L., and London, J. (1962) The low-level jet as related to nocturnal thunderstorms over the midwest United States, J. Appl. Meteorol. 1:43-47.

56. Bonner, W.D. (1968) Climatology of the low-level jet. Mon. Wea. Rev. 96:833-850.

57. Harclerode, P. (1986) GQ's 8 metre low-level parachute, Special Force Journal 1(No. 1).

58. Scorer, R.S. (1955) Theory of airflow over mountains: IV-Separation of flow from the Surface, Quart. J. Roy. Meteorol. Soc. 81:340-350.

59. Scorer, R.S. (1972) Clouds of the World, Stackpole Books, Harrisburg, PA.

60. Jones, O.K. (1970) The flow of a stratified fluid over a vertical step, Tellus 22(5):481-492.

61. Orgill, M.M. (1981) Atmospheric Studies in Complex Terrain: A Planning Guide for Future Studies, PNL-3656, ASCOT/80/4, Pacific Northwest Laboratory, Richland, Wash., 99352.

Appendix A

Description of Turner Drop Zone Case Studies

This appendix is structured in the following manner:

(1) Summary of 1200Z synoptic situation for each case, to include relevant surface features (for example, fronts, highs, lows, and so on), predominant surface and upper-level (500-mb) flows, with information about precipitation during the previous 24 h.
(2) Discussion of input to model (cloud cover/type/level, visibility, temperature, winds), plus any relevant information concerning multiple model runs, choice of runs, and so on.
(3) Discussion of conditions at Turner DZ for each operational case.

For Cases 2 and 3, the synoptic discussion covers the period from the preceding 1200Z analysis to the following 1200Z analysis.

Case 1 — 17 September 1800Z

Synoptic Situation - High-pressure ridge from northern Quebec to mid-Atlantic states. Light northwesterly flow over New England. Dry northwest flow over the northeast at 500 mb. Light precipitation recorded over eastern half of Massachusetts from previous 24 h.

Input Conditions - Used 11Z TAF to initialize model. Forecast from TAF: 2/8 Sc 050, 7 + mi vsby, 65°F, 330°/5 kt.

DZ Conditions - Paradrop may by C-130 aircraft carrying about 10 troops. Flight level was about 800 to 1000-ft AGL, aircraft approach from 289° (meteorological direction). Jumpers were taken by wind towards the southeast, and one jumper landed close to trees at eastern edge of DZ.

Case 2 – 17 October 0100Z

Synoptic Situation (Using 16 October and 17 October charts) - Weakening cold front moved from northern plains and Great Lakes to Ohio River Valley. Associated low and cold front moved from north of Lake Huron to western Pennsylvania and New York City area. High pressure located over Ontario - Manitoba border moved east to Lake Superior and western Quebec. Light and variable flow over New England became northerly after frontal passage. Trough at 500-mb centered about 85 W shifted to about 80°W as several short waves moved through flow. No precipitation during period over Massachusetts.

Input Conditions - Used 17Z 16 October TAF to initialize model. Forecast conditions: 5/8 Sc 035 F/8 Ac 100 8/8 Cs 250, 7 + mi vsby, 46°F, 290°/5 kt.

DZ Conditions - Balloon ascent showed direction about 295° over lowest several hundred feet before beginning to drift towards the south. Paradrop from two C-130s flying between 1000 ft and 1100 ft AFL. About four runs were made by each aircraft, dropping about eight to nine troops per run. Several different approach directions (from 250° to 295°) produced cross-wind components to jumpers causing both the marker panels and aircraft paths to be adjusted after the first run (when several troops drifted too close to eastern edge of DZ). Drops were made between about 0040 and 0130Z. Most jumpers experienced a southward drift due to prevailing winds (see Table 8).

Case 3 – 18 October 0630Z

Synoptic Situation (Using 18 October 1200Z charts) - High pressure centered over Lake Huron. Northerly to northwesterly flow over New England. Sharp 500-mb trough over New England. Light precipitation fell over much of northeast during previous 24 hr.

Input Conditions - Used 17Z Oct TAF for input. Forecast conditions: 7/8 Sc 035 4 Ac 080, 7 + mi vsby, 38 F, 010 /5 kt.

DZ Conditions - Balloon launch showed an almost vertical rise due to light winds. Wind direction was uniform from north-northeast most of way, turning to northeast near top of layer. Paradrop from C-130 flying at standard drop altitude. Aircraft made five runs across DZ before dropping troops on sixth run. About six drops were made from 0650 to 0730Z. Thirty-eight National Guardsmen made the jump, and despite the light winds, several who rode with the wind (recall Figure 16) came down quite rapidly.

Case 4 — 24 October 1800Z

Synoptic Situation - Series of high pressure cells extended from British Columbia through Ontario. Weak stationary front from southern Iowa eastward to Pennsylvania, becoming cold front off Delaware Peninsula. Light northwesterly flow over New England. Strong cyclonic flow at 500 mb around trough located off New England coast. Precipitation had occurred over Massachusetts during period.

Input Conditions - Used 11Z TAF to initialize model. Forecast conditions: 1/8 Ac 100 2/8 Ci 250, 7 + mi vsby, 57°F 350°/5 kt, wind 350°/10-15 kt 14-00Z. Model runs made first for 350°/5 kt, then for 350°/10 kt (from TAF remark). We decided to use second model run for verification on the basis of 5-6 kt winds reported at Moore AAF that morning.

DZ Conditions - Balloon showed strong winds between 100' and 500' AGL, then decreasing above 500' to produce MEW of 320°/12 kt. Personnel at DZ (SOWT and DZSO) have seen this type of speed profile before; however, no problems occurred during course of the jump from C-130 of approximately 60 troops from 900 to 1000 ft AGL. It is possible that strong low-level winds recorded by balloon could have been due to transient turbulent eddies, as evidenced by the surface gustiness of the wind this day. Jumps were made from 1815 to 1900Z, and again from 2000 to 2100Z. At 2000Z, Moore AAF recorded winds of 360°/6 kt with gusts to 13 kt.

Case 5 — 26 October 1500Z

Synoptic Situation - Cold front over northern New England, developing warm front over mid-Atlantic states, with light rain moving into southern New England from southwest. Very light winds over the region. Ridge at 500 mb over New York and New Jersey with westerly flow over New England.

Input Conditions - Since no TAF was available on the weekend, we used a combination of current regional observations to initialize the model. Aware of the wind problems at the airfield (they were open for observations), we surveyed nearby stations and found them all to have light winds, with ORH (Worcester, Massachusetts) reporting a direction of 350°. Input conditions were as follows: 8/8 As 100, 6 mi vsby, light rain and fog, 46°F, 350°/1 kt.

DZ Conditions - Balloon launch indicated very little wind until 2000 to 3000 ft AGL. Paradrop of about 40 troops from C-130 took about 45 minutes. One injury occurred, but was not weather-related.

Cases 6 and 7 — 28 October 1300Z, 1500Z

Synoptic Situation - Cold front was located about 500 km offshore. Weak high pressure ridge from Quebec to Ohio River Valley. Light and variable flow over New England. Trough at 500 mb from New York to North Carolina, and a jet streak moving over New England. Light precipitation had fallen over northeastern third of U.S. during period.

Input Conditions - Used 18Z 27 October TAF for input. Runs were made previous day. Forecast conditions prior to 13Z: 8/8 St 012, 1/2 mi vsby in fog, 51°F, 300°/5 kt. Conditions after 13Z: 4/8 St 012 5/8 Sc 030, 3 mi vsby in fog, 51°F, 330°/8 kt. Model runs were made using conditions prior to, and after 13Z, respectively. The first run was used for 13Z verification, while the second run was made for 15Z verification.

DZ Conditions. First balloon launch at 1300Z showed light winds until 200 to 300 ft, when it began to accelerate, indicating higher windspeeds from 300 ft to flight altitude. Paradrop from Army Blackhawk helicopter was delaved from 13Z to 15Z because of fog at Moore AAF. The balloon launched at 15Z showed a more uniform wind distribution with height. Paradrop of about 42 troops lasted from 1520 to 1645Z. No problems during operation until last jump when one jumper landed in trees because he did not turn into the wind soon enough. A second jumper landed on the dirt road close to DZ entrance. By the last two jumps, the surface winds had increased to 12 kt with stronger gusts. We suggest that strong vertical mixing was beginning to bring down stronger winds from aloft at this time. This observation is supported by the 13Z and 15Z balloon tracks, that changed from non-uniform to uniform wind conditions, and by the appearance of a broken Sc deck at 3000 ft at 17Z.

Case 8 - 29 October 1900Z

Synoptic Situation - High pressure off Virginia coast. Cold front approaching from Great Lakes. Southwesterly flow in advance of front over New England. Southwest flow at 500 mb over New England through flat ridge just off coast. Spotty precipitation over Massachusetts during previous period.

Input Conditions - Two model runs were made, using the 18Z 28 October and 12Z 29 October TAFs, respectively. Forecast conditions from first TAF: 4/8 Sc, 7 + mi vsby, 68°F, 240°/10 kt. Forecast from second TAF: 2/8 Sc 040 2/8 Ci 250, 7 + mi vsby, 68°F, 270°/6 kt. We chose to use the first model run on the basis of the winds observed over the region that morning (around 16Z), which were southwesterly with speeds of 7 to 15 kt.

DZ Conditions - Balloon track showed direction about 210° below 300 ft, shifting to 250° above 300 ft with a steady increase in speed. We computed MEWs for the following levels: 0 to 500 ft, 250°/11 kt; 0 to 1000 ft, 250°/13 kt; 0 to 1250 ft, 250°/14-15 kt. Gusty surface winds were observed over the DZ at this time. Jump scheduled from C-7 aircraft was cancelled due to mechanical problems. We believe it may have been just as well considering the strong wind conditions at the DZ.

Cases 9 and 10 — 30 October 1430Z, 1630Z

Synoptic Situation - Weakening cold front was just passing through the Ft. Devens area at 1200Z. Northwest flow was behind the front. Strong west to southwest flow at 500 mb accompanied this system. Precipitation was confined to New York and northern New England with this system.

Input Conditions - We made two model runs using the 12Z TAF for this case. The first run used pre-frontal conditions; the second run used post-frontal conditions (at 17Z). Pre-frontal forecast: 2/8 Sc 035, 7 + mi vsby, 59°F, 240 to 270°/4 kt. Post-frontal forecast: 2/8 Sc 035, 7 + mi vsby, 60°F, 290°/12 kt. It was obvious from the surface analysis that the frontal passage had already taken place by 12-13Z. We therefore used the post-frontal run (time of 17Z) for verification. The model horizontal wind plot for this case showed isolated areas of 15 kt winds over the DZ.

DZ Conditions - Balloon launch at 1415Z showed steady low-level winds becoming lighter above 1000 ft AGL. Gusty surface winds (peak gust of 19 kt at 1530Z) hindered Blackhawk jump operations for about 45 troops from 1520 to 1630Z, even causing several passes to be held until the gusts subsided. A second balloon was launched at 1640Z by Rhode Island Air National Guardsmen for C-130 cargo/equipment drop. Mean effective winds were calculated at different levels for this launch: 0 to 600 ft, 320°/9 kt; 0 to 800 ft, 320°/9 kt, 0 to 1100 ft, 320°/12 kt. Winds at Moore AAF were 330°/7 kt with gusts to 12 kt at 16Z.

Case 11 — 3 November 1800Z

Synoptic Situation - High pressure centered over northern New England. A ridge of high pressure extends southwestward into the southern Great Plains. An approaching frontal system is moving into the Great Lakes. Light and variable surface flow exists over New England. A strong westerly jet at 500 mb extends from the Great Lakes eastward into the Canadian Maritime Provinces. Light precipitation has fallen over all of Massachusetts during the previous 24 h.

Input Conditions - Used 12Z TAF to initialize model. Forecast conditions: 1/8 Sc 050, 7 + mi vsby, 51°F, 180°/7 kt after 16Z.

DZ Conditions - Balloon showed fairly moderate winds through the lowest layers, becoming lighter above 700 to 750 ft. Paradrop of eight troops from C-130 took place around 1835Z, with no problems encountered.

Case 12 — 5 November 1800Z

Synoptic Situation - Strong high pressure over the Canadian border area of New England. The ridge extends southward into the mid-Atlantic states, where a stationary front lies east-west from Cape Hatteras, North Carolina to a low in northwestern Mississippi. Overrunning precipitation associated with the stationary front extends from the Mississippi River Valley eastward into central New Jersey. Surface flow over New England is northerly, and the 500-mb flow is from the west-southwest ahead of a short-wave trough in Missouri. Light precipitation has fallen over Massachusetts during the previous 24 h.

Input Conditions - Used 12Z TAF to initialize model. Forecast conditions from TAF: 5/8 Ac 080 7 Cs 250, 7 + mi vsby, 39°F, 040°/7 kts; 17-18Z: 5/8 Ns 030, 5 mi vsby in light fog and rainshowers, 35°F, 090°/7 kt; 19-20Z: 8/8 Ns 010, 3 mi vsby in light intermittent rain, 35°F, 100°/10 kt. Information from the TAF for 18Z and later was used in determining input conditions. We made two model runs: one using the pre-17Z conditions, and the second using the 17-18Z conditions. Indications in the late morning (15Z) were that the pre-17Z conditions would remain over the area at jump time, so this forecast was used for verification.

DZ Conditions - Balloon track showed light northeast winds below 200 to 250 ft, changing to light easterly winds above. Paradrop from C-130 of about 40 troops occurred between 1820Z and 1850Z. Wind drift of troops was slight, even for those riding with the winds.

Case 13 — 7 November 1900Z

Synoptic Situation - Strong high pressure is centered over the Connecticut shore. The ridge extends from Nova Scotia into the southern Appalachian mountains. Surface flow is light and variable over New England, and west to southwesterly flow at 500 mb over the northeast exists in an area of weak ridging from New England southward to the mid-Atlantic states. Some substantial precipitation amounts (in excess of 0.25 in.) were recorded over Massachusetts during the previous 24 h, and snow fell through northeastern New York and most of Vermont, New Hampshire and Maine.

Input Conditions - Used 12Z TAF to initialize model. Forecast conditions: 2/8 St 010 7/8 St 023, 5 mi vsby in light fog, 50°F, variable winds at 5 kt; 17-18Z: 4/8 Sc 045, 7 + mi vsby, 57°F, 150°/7 kt. Model runs were made from both forecasts, using an 18Z time. In late morning (around 15Z), we decided to use pre-17Z forecast conditions for verification. We used a 220° wind direction for the first run based on observations at Worcester.

DZ Conditions - Balloon track showed southwest winds through the lowest 350 ft, becoming west-southwest above this level. Wind speeds remained fairly uniform throughout the layer. Paradrop from C-130 of approximately 30 paratroopers took place between 1900 and 1945Z (original time was supposed to be 1800Z). Winds were not a factor during this operation, even though there was one injury. Aircraft flight track was from 310 to 320° during this jump, which could have exposed the jumpers to strong cross winds if the winds has been stronger.

Appendix B

List of Acronyms and Symbols

AAF - Army Air Field

AFGL - Air Force Geophysics Laboratory

AFSC - Air Force Systems Command

AGL - Above Ground Level

ASL - Atmospheric Sciences Laboratory (Army)

AWS - Air Weather Service

Det - Detachment

DZ - Drop Zone

GMT - Greenwich Mean Time

MEW - Mean Effective Wind

MSL - Mean Sea Level

NBC - Nuclear, Biological, Chemical

NCAR - National Center for Atmospheric Research

NRC - Nuclear Regulatory Commission (US)

NWP - Numerical Weather Prediction

PBL - Planetary Boundary Layer

PE - Primitive Equation(s)

RAM - Random Access Memory

SOWT - Special Operations Weather Team (Air Force)

SP - Stability Parameter

TAF - Terminal Aerodrome Forecast

TFRN - Terminal Forecast Reference Notebook

TOT - Time on Target

USAFETAC - US Air Force Environmental Technical Applications Center

Z - "Zulu" Time (same as GMT)

5WS - Fifth Weather Squadron (AWS)

5WW - Fifth Weather Wing (AWS)

10th Group - US Army 10th Special

Cloud Types

Ci - Cirrus

Cs - Cirrostratus

Ac - Altocumulus

As - Altostratus

Sc - Stratocumulus

Ns - Nimbostratus

St - Stratus

END

DATE

3-88

DTIC